Computers and Structures 112-113 (2012) 217–234

Contents lists available at SciVerse ScienceDirect

Computers and Structures

journal homepage: www.elsevier.com/locate/compstruc

A generalized adaptive finite element analysis of laminated plates

P.M. Mohite *, C.S. Upadhyay

Department of Aerospace Engineering, Indian Institute of Technology Kanpur, Kanpur 208 016, India

ARTICLE INFO

Article history:
Received 21 February 2012
Accepted 19 August 2012

Keywords:
A-posteriori error estimation
Modeling error
Goal based adaptivity
Explicit modeling error indicator
Laminate models

ABSTRACT

A generalized approach for adaptive finite element analysis of laminated composite structures is presented in this study. The approach quantifies and controls discretization and modeling error. The goal of this paper is to present an economical, easily computable and relatively robust error estimator. A patch recovery based discretization error estimator is used and a goal based one shot adaptive procedure is implemented to control the discretization error. An explicit indicator, for estimation of modeling error, has been proposed for the laminated composites. The quality of the discretization and modeling error estimators is studied through numerical examples. The effectiveness of the proposed approach is also demonstrated through the analysis of damaged laminates. The key advantage of the proposed approach is that the desired mesh and models in the laminate are adapted automatically to achieve the user specified error tolerances in discretization and modeling errors.

1. Introduction

Let us introduce the terminology for various solutions of the system of laminated plates as:

$\mathbf{u}_{3D}$	the exact (three dimensional) solution to the problem considered
$\mathbf{u}^M$	the exact solution for the model considered
$\mathbf{u}^{M,h}$	the finite element solution of the model

Then the error between the exact solution and finite element solution ("total error") is given as:

$$\text{total error} = \mathbf{u}_{3D} - \mathbf{u}^{M,h} = \mathbf{u}_{3D} - \mathbf{u}^M + \mathbf{u}^M - \mathbf{u}^{M,h} = (\mathbf{u}_{3D} - \mathbf{u}^M) + (\mathbf{u}^M - \mathbf{u}^{M,h}) \quad (1)$$

The first bracketed term on the right hand side denotes the error in the exact solution of the actual problem and exact solution of the model used; second term denotes the error in the exact solution of the model and its finite element approximation. The first term is called the "modeling error" ($\mathbf{e}^M$) and second term is the "discretization error" ($\mathbf{e}^{M,h}$). Thus,

$$\text{total error} = \mathbf{e}^M + \mathbf{e}^{M,h} \quad (2)$$

Using triangle inequality, the total error (in some norm) is given as

$$\|\text{total error}\| = \|\mathbf{u}_{3D} - \mathbf{u}^{M,h}\| \leqslant \|\mathbf{u}_{3D} - \mathbf{u}^M\| + \|\mathbf{u}^M - \mathbf{u}^{M,h}\| \quad (3)$$

Thus, Eq. (2) means that a proper analysis would require simultaneous control of modeling and discretization error. In this study, it is assumed that an appropriate (plate) model is chosen. This plate model is fixed and the discretization error will be measured with respect to the exact solution of the fixed plate model.

A number of methodologies are available in literature for estimation and control of discretization error (for example, see [1] and references therein and [2,3]). Smoothening based a-posteriori error estimators are found to be robust, computationally economical and easily implementable (see [4,5] for example). Several alternative versions of smoothening based discretization error estimators are proposed by the authors [6–10] for laminated composites. A detailed review on a-posteriori error estimation can also be found in [11].

The hierarchic modeling approach has become very popular in recent years (see [12] for example). The idea of hierarchic model is to connect these models together in some way such that an appropriate level of sophistication is obtained for a given accuracy. This concept has led to the, so called, *q* or model adaptivity. A *q* adaptivity method for selecting optimal hierarchical models has been studied by Vogelius and Babuška [13] and Babuška and Schwab [14] for two-dimensional scalar field problems. A-priori modeling error estimator was proposed by Oden and Cho [15] for hierarchic model for plate and shell like structures. The orthogonality property of modeling and discretization errors was used to get the error estimate. Stein et al. [16] have developed *hd* adaptive modeling scheme for elastic structures. Further, in [17,18] they have proposed coupled model and solution adaptivity using subdomain residual method which uses a-posteriori equilibrium method for the calculation of the interface tractions.

* Corresponding author. Tel.: +91 512 2596024; fax: +91 512 2597561/7626.
E-mail address: mohite@iitk.ac.in (P.M. Mohite).

0045-7949/$ - see front matter © 2012 Elsevier Ltd. All rights reserved.
http://dx.doi.org/10.1016/j.compstruc.2012.08.002

Oden et al. [19] have extended the concept of hierarchical modeling to heterogeneous materials. Further, goal-oriented adaptive modeling for heterogeneous solid is proposed in [20,21]. The derivation and analysis of a-posteriori modeling error estimators for hierarchic models of homogeneous and elastic plates is done by Schwab [22]. The computable modeling error estimators are derived for monoclinic materials using the residual tractions on the faces of the plate. Similar approach has been used for heat conduction problem in plates by Babuška and Schwab [23]. Further, this approach allows simultaneous use of different model orders in various subregions (see [24] also). A review on modeling error estimation can be seen due to Oden and Prudhomme [25].

The goal of this paper is to give a methodology for accurate and economical computation of various quantities of interest, like stress and displacement at a point in the laminated composite structures. Families of plate models are studied for their accuracy. A region-by-region modeling approach [26,27], where any model can be put in any region of the domain, along with goal based adaptive method [7] to control the discretization error, is presented. Further, an explicit modeling error estimator for laminated plates for adaptive modeling strategy is proposed.

2. Plate models

Several families of plate models have been proposed in the literature (for example, see [12]) for the analysis of homogeneous and laminated plates. These families can be broadly categorized as (a) shear deformable theories, (b) zig-zag theories and (c) layer-by-layer or three dimensional theories.

The plate models used in this study are based on generalized forms of the shear deformable theories and layer-by-layer theories. In general, the models proposed in the literature are for bending dominated problems. For such problems it can be shown that the transverse displacement is symmetric (with respect to the depth coordinate z) while the in-plane displacements are antisymmetric (see [22]). However, this is true only for symmetric laminates. For other cases (e.g. anti-symmetric and unsymmetric laminates), the deformation has both bending and membrane components. This requires a general representation of the displacement field (through the thickness). In the following, we outline the two families of generalized plate models which are used in this study.

2.1. Layerwise and equivalent plate models

2.1.1. Layerwise plate model (LM)

This is the most general three-dimensional representation of the displacement field. The transverse functions $\overline{M}_i(z)$ are defined as the one dimensional basis functions over each lamina. From Fig. 1(b), it can be seen that the representation of the displacement field is given by:

$$\begin{aligned} u(x,y,z) &= \sum_{i=1}^{n_1} u_i(x,y)\overline{M}_i(z) \\ v(x,y,z) &= \sum_{i=1}^{n_2} v_i(x,y)\overline{M}_i(z) \\ w(x,y,z) &= \sum_{i=1}^{n_3} w_i(x,y)\overline{M}_i(z) \end{aligned} \tag{4}$$

where u_i, v_i and w_i are the in-plane (unknown) functions in x, y and z directions, respectively. $n_1 = n_2$ and n_3 are the number of nodes in the laminate thickness direction and depend on the transverse order of approximation $p_z^u = p_z^v,\ p_z^w$ for the displacement components in x, y and z directions, respectively and the number of laminae (or layers) nl in the laminate. Hence, here the number of unknowns grows with the number of laminae. The exact solutions corresponding to this family of models will be given as $LMp_z^u p_z^v p_z^w$. The corresponding finite element solutions will be represented by $LMp_{xy}p_z^u p_z^v p_z^w$, where p_{xy} is the order of in-plane approximation. For example, $LM2330$ corresponds to the layerwise model with $p_{xy} = 2$ and $p_z^u,\ p_z^v = 3,\ p_z^w = 0$.

2.1.2. Equivalent plate model (EQ)

These are generalized versions of the shear deformable theories. As compared to shear deformable theories, any higher order representation of both the in-plane and transverse displacement components can be done, with respect to the z-coordinate.

The transverse functions are shown in Fig. 1(a) as an example. Generally $p_z^u = p_z^v$ is chosen. For this model, $n_1 = p_z^u + 1, n_2 = p_z^v + 1$ and $n_3 = p_z^w + 1$. Here, n_1, n_2 and n_3 denote the number of nodes in the laminate thickness direction. The exact solutions corresponding to this family of models will be given by $EQp_z^u p_z^v p_z^w$ and the corresponding finite element solutions will be represented by $EQp_{xy}p_z^u p_z^v p_z^w$. For example, $EQ3110$ corresponds to the equivalent model with $p_{xy} = 3$ and $p_z^u,\ p_z^v = 1,\ p_z^w = 0$.

Note that in Fig. 1(a) a quartic transverse approximation over a laminate is shown whereas in Fig. 1(b) a cubic approximation over each layer is shown. In the present study up to quartic transverse approximation for the displacement field is used. In the following, $\mathbf{u}$ will be used to represent the exact three-dimensional solution $\mathbf{u}_{3D}$, while $\mathbf{u}^M$ will denote the exact solution of a chosen model.

It should be noted that many of the conventional higher order shear deformable laminated plate theories can be represented using this model. Here, we have not considered the zig-zag theories. This class of models ensures that the computational cost is independent of the number of layers in the laminate.

An exhaustive work on laminated plates and shells can be seen in [28]. A detailed review of zig-zag theories can be seen in [29]. More literature on plate models can be seen in references therein.

For the sake of simplicity, the generic plate model will be defined as:

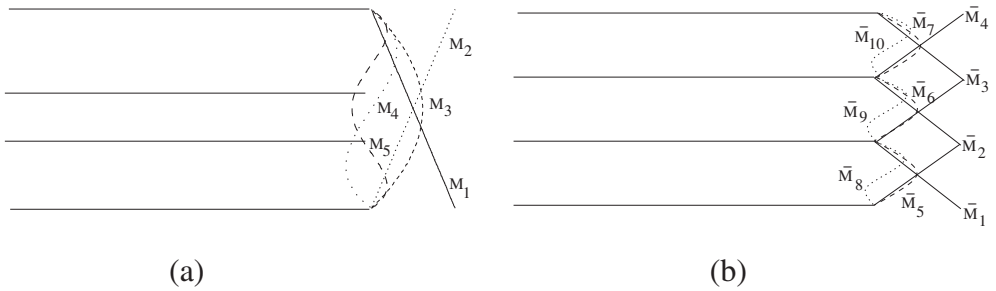

Fig. 1. Transverse approximation for (a) equivalent model: example of 4th order transverse approximation; (b) layerwise model: example of cubic order transverse approximation.

$$\mathbf{u}^M(x,y,z) = \left\{ \begin{array}{c} u_M(x,y,z) \\ v_M(x,y,z) \\ w_M(x,y,z) \end{array} \right\} = [\phi(z)]_M \, \mathbf{U}^M(x,y) \tag{5}$$

where $[\phi(z)]_M$ corresponds to the z-transverse functions used and $\mathbf{U}^M(x,y)$ are the corresponding in-plane (unknown) functions. In the finite element analysis, the approximate solution $\mathbf{u}^{M,h}$ has the form (5), with $\mathbf{U}^M(x,y)$ replaced by $\mathbf{U}^{M,h}(x,y)$ and given by

$$U_i^{M,h}(x,y) = \sum_{k=1}^{nd_i} u_{ik}^M \Psi_k(x,y) \tag{6}$$

where $\Psi_k(x,y)$ are the two-dimensional basis functions of given order p_{xy}, u_{ik}^M are the in-plane nodal displacement components and nd_i is the total number of terms in the expansion.

2.2. Region-by-region plate model (RR)

The idea of region-by-region modeling approach is to put any model in any region of the domain. In the vicinity of cut-outs and outer boundaries of the domain the solution is expected to be unsmooth, have severe boundary layer effect, and possibly be three-dimensional in nature. Hence, along with a refinement of the mesh, enrichment of the model will also be desired in these regions. It was shown in [10,26,27] that layerwise models are very effective in capturing the three dimensional effects at these structural details while elsewhere equivalent single layer models with post-processed transverse stresses, that is the transverse stresses obtained using the equilibrium equations, can be used. The details of implementation of region-by-region model can be seen in [10,26,27].

3. Finite element formulation

The total potential, Π, for the structure is given by

$$\Pi(\mathbf{u}) = \frac{1}{2}\int_V \{\sigma(\mathbf{u})\}^T\{\varepsilon(\mathbf{u})\}\,dV - \int_{R^+\cup R^-} T_3 u_3 \, ds - \int_{\Gamma_N} (T_1 u_1 + T_2 u_2) ds \tag{7}$$

where V is the volume enclosed by the plate domain; $\{\sigma(\mathbf{u})\}$ and $\{\varepsilon(\mathbf{u})\}$ are the engineering stress and strain vectors, respectively. R^+ and R^- are the top and bottom faces of the plate and $T_3(x,y)$ is the applied transverse load on these faces; Γ are the lateral faces with $\Gamma = \Gamma_N \cup \Gamma_D$ and Γ_N = Neumann boundary, Γ_D = Dirichlet boundary; T_1, T_2 are the in-plane tractions specified on the lateral faces. Here, u_1, u_2 and u_3 denotes the three components of the displacement field $\mathbf{u}$. Using any of the model described by (5), the corresponding total potential $\Pi_M(\mathbf{u}^M)$ can be defined by substituting $\mathbf{u}$ with $\mathbf{u}^M$ in (7).

The approximate solution to the problem, $\mathbf{u}^{M,h}$, is the minimizer of the total potential $\Pi_M(\mathbf{u}^{M,h})$ and is obtained from the solution of the following weak problem:

Find $\mathbf{u}^{M,h} \in H_M^0(\mathbf{V})$ such that

$$\mathcal{B}(\mathbf{u}^{M,h}, \mathbf{v}^{M,h}) = \mathcal{F}(\mathbf{v}^{M,h}) \quad \forall\ \mathbf{v}^{M,h}\ H_M^0(\mathbf{V}) \tag{8}$$

where

$$\mathcal{B}(\mathbf{u}^{M,h}, \mathbf{v}^{M,h}) = \int_V \{\sigma(\mathbf{u}^{M,h})\}^T\{\varepsilon(\mathbf{v}^{M,h})\}\ dV,$$

$$\mathcal{F}(\mathbf{v}^{M,h}) = -\int_{R^+\cup R^-} T_3 v_3^{M,h}\ ds - \int_{\Gamma_N} \left(T_1 v_1^{M,h} + T_2 v_2^{M,h}\right) ds$$

and $H_M^0(\mathbf{V}) = \{\mathbf{v}^M | \Pi_M(\mathbf{v}^M) < \infty$ and $\mathcal{M}\ \mathbf{v}^M = \mathbf{0}$ on $\Gamma_D\}$; $\mathbf{v}^{M,h}$ is the test function and has the same form as $\mathbf{u}^{M,h}$ given by (5) and (6). We will further define $\sqrt{\mathcal{B}(\mathbf{v},\mathbf{v})} = \|\mathbf{v}\|_E$ as the energy norm. Note that $\mathcal{B}(\mathbf{u}^{M,h}, \mathbf{u}^{M,h}) = 2\mathcal{U}(\mathbf{u}^{M,h})$ where $\mathcal{U}(\mathbf{u}^{M,h})$ is the strain energy for the solution $\mathbf{u}^{M,h}$. Note that in this study Dirichlet means the part of lateral boundary where geometric constraints are imposed, while Neumann stands for the parts of the lateral boundary where in-plane traction is applied. Further, $\mathcal{M}$ is a generic representation of displacement constraints on the Dirichlet boundary edge. For example, the boundary conditions can be clamped $(u_i^M = 0,\ i = 1,2,3)$; soft simple-support $(u_n^M, u_3^M = 0)$; hard simple-support $(u_t^M, u_3^M = 0)$, etc. Here, u_n^M and u_t^M denote in-plane displacement normal and tangential to an edge, respectively.

Note that in the case of conventional models, integration through the depth leads to the (z averaged) weak formulation over the projected mid-plane.

Using direct finite element data it is easy to show that the strain energy for various plate models, for the same in-plane mesh and in-plane order of approximation p_{xy}, follows the relationship (when homogeneous conditions are specified on the Dirichlet boundaries):

$$\begin{aligned} &\mathcal{U}_{EQ\ p_{xy}110} \leqslant \mathcal{U}_{EQ\ p_{xy}112} \leqslant \mathcal{U}_{EQ\ p_{xy}332} \cdots \leqslant \mathcal{U}_{3D} \\ &\mathcal{U}_{EQ\ p_{xy}p_z^u p_z^v p_z^w} \leqslant \mathcal{U}_{LM\ p_{xy}p_z^u p_z^v p_z^w} \leqslant \mathcal{U}_{3D} \\ &\mathcal{U}_{LM\ p_{xy}110} \leqslant \mathcal{U}_{LM\ p_{xy}112} \leqslant \mathcal{U}_{LM\ p_{xy}332} \cdots \leqslant \mathcal{U}_{3D} \end{aligned} \tag{9}$$

In (9) $\mathcal{U}_{EQ\ p_{xy}110}$ stands for the strain energy corresponding to $EQp_{xy}110$ model; $\mathcal{U}_{LM\ p_{xy}332}$ stands for the strain energy corresponding to $LMp_{xy}332$ model; $\mathcal{U}_{3D}$ corresponds to strain energy $\mathcal{U}(\mathbf{u}_{3D})$, that is, for the exact three-dimensional solution. The other terms in this equation can be deduced similarly.

4. Discretization error estimation

Many classes of a-posteriori error estimators are available in the literature (see [1,3]). For the three-dimensional problems, the implicit type residual error estimators would prove to be computationally expensive. Hence, the more economical recovery (or projection) based error estimators have been employed in this study. It was found in [30–32] that the error estimator based on stress recovery (defined in [5]) was reliable locally for patches at the boundary of the domain, as well as the interior of the domain. Several definitions of such projections are possible (see [31,32]). Here, following [6,10], a simple L_2 projection based a-posteriori error estimator is developed for the displacement field.

4.1. L_2 projection based a-posteriori error estimator

Let us consider the three-dimensional mesh obtained by first meshing the mid-plane (using a two-dimensional mesh) and then extending the mesh in the thickness direction to give wedge-shaped elements in each layer. In the proposed implementation, irrespective of the plate model used, recovery will be done over the three-dimensional mesh.

For an element τ in the lth lamina, let P_τ be the patch of elements in a one-layer neighborhood of τ in the lth lamina, as shown in Fig. 2(a).

Over the patch P_τ, define the recovered displacement field $\mathbf{u}^{M,*}$

$$\mathbf{u}^{M,*} = \left\{ \begin{array}{c} u^* \\ v^* \\ w^* \end{array} \right\} = [\phi(z)]_M \, \mathbf{U}^{M,*}$$

where $U_i^{M,*}(x,y) = \sum_{j=1}^{N_{DOF}} A_{ij}\ q_j(x,y)$ with $N_{DOF} = (p_{xy}+k+1)(p_{xy}+k+2)/2$; $q_j(x,y)$ are the monomials of order $\leqslant p_{xy}+k, k \geqslant 1$ (see [6] for details).

The coefficients A_{ij} are obtained by minimizing

$$J_{2,\mathbf{U}^{M,*}} = \frac{1}{2}\int_{V_{P_\tau}} |\mathbf{U}^{M,*} - \mathbf{U}^{M,h}|^2 dV \tag{10}$$

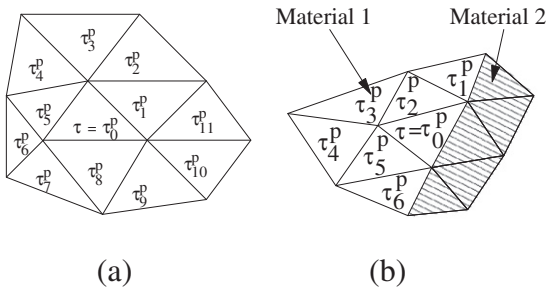

Fig. 2. Element τ with the patch P_τ (a) consisting of elements $\left\{\tau_i^{(P_\tau)}\right\}_{i=0,1,\ldots,11}$ of same material; (b) consisting of elements of two different materials.

where V_{P_τ} is the volume of the patch P_τ enclosed by the elements in P_τ. Further, A_{P_τ} is the projected area of the patch.

Remark. This is a generalization of the approach given in [6], such that for any model of choice (layerwise or equivalent), recovery can be done using the same recipe.

Following [6], a measure of the error (i.e. the desired "true error") is given as $\bar{\mathbf{e}}_h^M \approx \mathbf{u}^{M,h(p_{xy}+k)} - \mathbf{u}^{M,h(p_{xy})}$, where $\mathbf{u}^{M,h(m)}$ is the finite element solution obtained with elements of order m. In all the computations, reported in this study, $k = 1$ is used. Hence, a measure of the actual error is obtained by solving for another finite element solution over the same mesh, with in-plane order $\bar{p}_{xy} = p_{xy} + 1$. An approximation of the error is given by $\mathbf{e}_h^{M,*} \approx \mathbf{u}^{M,*} - \mathbf{u}^{M,h}$. Hence, the element error indicator η_τ is given as

$$\eta_\tau^2 = \int_{v_\tau^l} \{\sigma(\mathbf{u}^{M,*}) - \sigma(\mathbf{u}^{M,h})\}^T \{\varepsilon(\mathbf{u}^{M,*}) - \varepsilon(\mathbf{u}^{M,h})\} dV \tag{11}$$

where v_τ^l is the volume enclosed by the τth element in lth layer and $\{\sigma(\mathbf{u}^{M,*})\}$ and $\{\varepsilon(\mathbf{u}^{M,*})\}$ are the engineering stress and strain vectors, respectively obtained from the recovered displacement field $\mathbf{u}^{M,*}$. Now, given the element error indicator η_τ, the error estimator ξ_ω in a patch $\omega(\omega \subseteq V)$ is given as

$$\xi_\omega = \sqrt{\sum_{\tau=1}^{N_{EL,\omega}} \eta_\tau^2} \tag{12}$$

where $N_{EL,\omega}$ is the number of elements in the patch ω. The "desired" error norm will be $\|\bar{\mathbf{e}}_h^M\|_{E(\omega)} = \sqrt{2\,\mathcal{U}_\omega(\bar{\mathbf{e}}_h^M)}$, which will be used to obtain a measure of the quality of the error estimators, i.e.

$$\kappa_\omega = \frac{\xi_\omega}{\|\bar{\mathbf{e}}_h^M\|_{E(\omega)}} \tag{13}$$

where κ_ω is the effectivity index (the ideal value of κ_ω is 1).

Remark. When there is a material discontinuity or model discontinuity (as in region-by-region models), the averaging is done over the elements with same material or model (see Fig. 2(b)).

5. Focussed adaptivity

In the analysis of layered media, often the goal is to obtain stress or strain in the material directions in a lamina or at an interface, in the critical regions. These quantities may be used in a damage initiation [33] or damage growth model (for example see [34]), to predict onset and propagation of damage. Hence, local quantities have to be accurately obtained. In order to do this, several goal-based error estimators [1,9,11], and adaptive procedures have been proposed in the literature (see [1–3]). Following [1], it can be shown that error in the quantity of interest can be obtained by solving an auxiliary problem. Below, the definition of the auxiliary problem is given for the layered media.

Remark. In this section the 'error' refers to 'discretization error' and 'error estimator' refers to 'discretization error estimation'.

5.1. The auxiliary problem

Let us consider the domain of Fig. 3(a). Fig. 3(b) shows the global and principal material directions for a lamina. Let us further assume that the value of strain component ε_{xx} in the topmost layer is the quantity of interest, for all points in the element τ (shown shaded in Fig. 3(a)). In order to accurately obtain the pointwise information in τ, let

$$\varepsilon_{xx,avg}^{(l)} = \frac{1}{v_\tau^l} \int_{v_\tau^l} \varepsilon_{xx} dv$$

be the quantity of interest. Here, $v_\tau^l = A_\tau t_l$ is the volume enclosed by the element τ in the lth layer. Hence,

$$\varepsilon_{xx,avg}^{(l)} = \frac{1}{A_\tau t_l} \int_{z=z_{l-1}}^{z_l} \int_{A_\tau} (\varepsilon_{xx}\, dA) dz \tag{14}$$

with t_l is the thickness of the lth layer; z_{l-1} and z_l are the lower and upper z coordinates for the lth layer; A_τ is the area of element τ.

Corresponding to $\varepsilon_{xx,avg}^{(l)}$ define the following auxiliary problem:

Find $\mathbf{G}^M \in \mathbf{H}_M^0(\mathbf{V})$ such that

$$\mathcal{B}(\mathbf{G}^M, \mathbf{v}^M) = \varepsilon_{xx,avg}^{(l)}(\mathbf{v}^M) = \mathcal{F}(\mathbf{v}^M) \quad \forall \mathbf{v}^M \in \mathbf{H}_M^0(\mathbf{V}) \tag{15}$$

Letting $\mathbf{G}^{M,h} \in \mathbf{H}_M^0(\mathbf{V})$ be the finite element solution for $\mathbf{G}^M$ such that

$$\mathcal{B}(\mathbf{G}^{M,h}, \mathbf{v}^{M,h}) = \varepsilon_{xx,avg}^{(l)}(\mathbf{v}^{M,h}) = \mathcal{F}(\mathbf{v}^{M,h}) \quad \forall \mathbf{v}^{M,h} \in \mathbf{H}_M^0(\mathbf{V}) \tag{16}$$

Note that definition (15) is used to regularize the function $\mathbf{G}^M$, ensuring that it lies in $\mathbf{H}_M^0(\mathbf{V})$. For more details see [1].

5.2. Estimators for error in quantity of interest

From Eqs. (15) and (16) it follows that

$$\mathcal{B}(\mathbf{G}^M, \mathbf{u}^M - \mathbf{u}^{M,h}) = \mathcal{F}(\mathbf{u}^M) - \mathcal{F}(\mathbf{u}^{M,h}) = \mathcal{F}(\mathbf{u}^M - \mathbf{u}^{M,h}) = \mathcal{F}(\mathbf{e}^{M,h}) \tag{17}$$

From the orthogonality property of the error (for the self-adjoint problems) in the finite element solution

$$|\mathcal{B}(\mathbf{G}^M - \mathbf{G}^{M,h}, \mathbf{u}^M - \mathbf{u}^{M,h})| = |\mathcal{F}(\mathbf{e}^{M,h})| \tag{18}$$

or

$$\begin{aligned} |\mathcal{F}(\mathbf{e}^{M,h})| &= |\mathcal{B}(\mathbf{G}^M - \mathbf{G}^{M,h}, \mathbf{u}^M - \mathbf{u}^{M,h})| \\ &\leqslant \sum_\tau |\mathcal{B}(\mathbf{G}^M - \mathbf{G}^{M,h}, \mathbf{u}^M - \mathbf{u}^{M,h})| \\ &\leqslant \sum_\tau \|\mathbf{e}_\mathbf{u}^M\|_{E(\tau)} \, \|\mathbf{e}_{\mathbf{G}^M}\|_{E(\tau)} \leqslant \|\mathbf{e}_\mathbf{u}^M\|_{E(\Omega)} \|\mathbf{e}_{\mathbf{G}^M}\|_{E(\Omega)} \end{aligned} \tag{19}$$

where $\mathbf{e}_\mathbf{u}^M = \mathbf{e}^{M,h}$ stands for the error in the actual solution and $\mathbf{e}_{\mathbf{G}^M}$ stands for the error in the auxiliary problem, $\|\cdot\|_{E(D)}$ stands for energy norm in the domain D. Thus, it can be seen that the smoothness of both $\mathbf{u}^M$ and $\mathbf{G}^M$ affect the measure of error in the quantity of interest.

Following [7,26] the error estimators for the local quantity of interest were proposed. However, in the present study following [7,26] the error estimator used is given briefly.

Replacing $\mathbf{e}_\mathbf{u}^M$ with the estimate $\mathbf{e}_\mathbf{u}^{M,*}$ and $\mathbf{e}_{\mathbf{G}^M}$ with the estimate $\mathbf{e}_\mathbf{G}^{M,*}$, the following error estimator for the error in the quantity of interest is defined

$$|\mathcal{F}(\mathbf{e}^{M,*})| = \sum_\tau \left|\mathcal{B}\left(\mathbf{e}_\mathbf{u}^{M,*}, \mathbf{e}_\mathbf{G}^{M,*}\right)\right| \tag{20}$$

It is shown in [7,26] that this error estimator is reliable as compared to other error estimators defined therein.

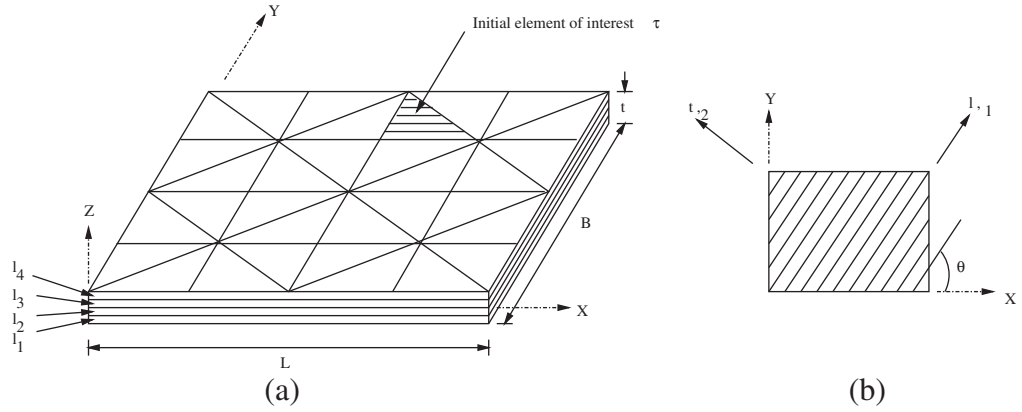

Fig. 3. (a) A laminated plate with initial mesh and element of interest τ with top and bottom faces and (b) global and material directions for a laminate.

Remark. The error estimator is robust with $0.8 \leqslant |\mathcal{F}(\mathbf{e}^{M,*})|/|\mathcal{F}(\mathbf{e}^{M,h})| \leqslant 2$ as shown in [7].

5.3. One-shot adaptivity for quantity of interest

Letting τ be the element of interest and P_τ the one-layer element neighborhood of τ, the total error can be partitioned into two parts as follows (see [30])

$$|\mathcal{F}(\mathbf{e}^{M,h})| \leqslant |\mathcal{F}_1(\mathbf{e}^{M,h})| + |\mathcal{F}_2(\mathbf{e}^{M,h})|$$

where

$$\mathcal{F}_1(\mathbf{e}^{M,h}) = \sum_{\tau\in P_\tau} \mathcal{B}\left(\mathbf{e}^{M,h}, \mathbf{e}_{\mathbf{G}^M}\right), \quad \mathcal{F}_2(\mathbf{e}^{M,h}) = \sum_{\tau\in P'} \mathcal{B}\left(\mathbf{e}^{M,h}, \mathbf{e}_{\mathbf{G}^M}\right) \tag{21}$$

Here P' is the set of elements lying outside P_τ. Following [40], $\mathcal{F}_1(\mathbf{e}^{M,h})$ is the local part of the error and $\mathcal{F}_2(\mathbf{e}^{M,h})$ is the "pollution" in the quantity of interest (i.e. far-field influence). Following [7,30,41],

$$|\mathcal{F}_1(\mathbf{e}^{M,h})| \leqslant \sum_{\tau\in P_\tau} \left\|\mathbf{e}^M_{\mathbf{u}}\right\|_{E(\tau)} \left\|\mathbf{e}_{\mathbf{G}^M}\right\|_{E(\tau)} \leqslant Ch^{p_{xy}} \tag{22}$$

Beyond P_τ, the auxiliary function is well behaved and hence

$$\left|\mathcal{F}_2\left(\mathbf{e}^{M,h}_h\right)\right| \leqslant \sum_{\tau\in P'} \left\|\mathbf{e}^M_{\mathbf{u}}\right\|_{E(\tau)} \left\|\mathbf{e}_{\mathbf{G}^M}\right\|_{E(\tau)} \leqslant Ch^{2p_{xy}} \tag{23}$$

The goal of the adaptive process is to refine the given mesh selectively such that the total error is below the specified tolerance, i.e.

$$|\mathcal{F}(\mathbf{e}^{M,h})| \leqslant \Theta|\mathcal{F}(\mathbf{u}^{M,h})| \tag{24}$$

where $\mathcal{F}(\mathbf{u}^{M,h})$ is the computed value of the desired quantity of interest. Following [42], $r_\tau = \frac{h_d}{h}$ is defined as the ratio of the desired (h_d) to the actual mesh size (h) of the element τ. The desired mesh should have the least number of elements, of all possible meshes. Hence, following [42], the quantity

$$\sum_\tau \frac{1}{r_\tau^2}$$

is minimized subject to constraints (22) and (23). Thus, the new objective function (to be minimized) is defined as,

$$L = \sum_\tau \frac{1}{r_\tau^2} + \lambda_1\left(\sum_{\tau\in P_\tau} \chi^2_{d,\tau} - \mathcal{F}_{d,1}\right) + \lambda_2\left(\sum_{\tau\in P'} \chi^2_{d,\tau} - \mathcal{F}_{d,2}\right) \tag{25}$$

where $\chi_{d,\tau} = |\mathcal{B}(\hat{\mathbf{e}}^M_{\mathbf{u}}, \hat{\mathbf{e}}_{\mathbf{G}^M})|$ is the desired contribution to the total error from element τ; $\hat{\mathbf{e}}^M_{\mathbf{u}}$, $\hat{\mathbf{e}}_{\mathbf{G}^M}$ are the desired errors in the element τ; λ_1 and λ_2 are Lagrange multipliers; $\mathcal{F}_{d,1} = \Theta_1|\mathcal{F}(\mathbf{u}^{M,h})|$ and $\mathcal{F}_{d,2} = \Theta_2|\mathcal{F}(\mathbf{u}^{M,h})|$ are the desired errors in the region P_τ and P', respectively (here $\Theta = \Theta_1 + \Theta_2$). Using (22) and (23) $\chi^2_{d,\tau}$ can be given in terms of the actual error $\chi^2_{a,\tau}$ (where $\chi^2_{a,\tau} = |\mathcal{B}(\mathbf{e}^M_{\mathbf{u}}, \mathbf{e}_{\mathbf{G}^M})|$ in the element τ), as

$$\text{For} \quad \tau \in P_\tau, \quad \chi^2_{d,\tau} = r_\tau^{p_{xy}} \chi^2_{a,\tau}$$

$$\text{For} \quad \tau \in P', \quad \chi^2_{d,\tau} = r_\tau^{2p_{xy}} \chi^2_{a,\tau}$$

Thus, (25) becomes

$$L = \sum_\tau \frac{1}{r_\tau^2} + \lambda_1\left(\sum_{\tau\in P_\tau} r_\tau^{p_{xy}} \chi^2_{a,\tau} - \mathcal{F}_{d,1}\right) + \lambda_2\left(\sum_{\tau\in P'} r_\tau^{2p_{xy}} \chi^2_{a,\tau} - \mathcal{F}_{d,2}\right) \tag{26}$$

Minimizing L with respect to r_τ, λ_1 and λ_2 gives the desired mesh sizes (see [7–9] for details).

For $\tau \in P_\tau$,

$$r_\tau = \frac{\mathcal{F}_{d,1}^{1/p_{xy}}}{\left(\sum_{\tau\in P_\tau} \chi^{4/(p_{xy}+2)}_{a,\tau}\right)^{1/p_{xy}} \cdot \chi^{2/(p_{xy}+2)}_{a,\tau}} \tag{27}$$

and for $\tau \in P'$,

$$r_\tau = \frac{\mathcal{F}_{d,2}^{1/2p_{xy}}}{\left(\sum_{\tau\in P'} \chi^{2/(p_{xy}+1)}_{a,\tau}\right)^{1/p_{xy}} \cdot \chi^{1/(p_{xy}+1)}_{a,\tau}} \tag{28}$$

Remark. The partition of the contribution to the error from P_τ and P' depends on the user. The final mesh depends on the choice of Θ_1 and Θ_2. In order to keep both contributions of the same order, here $\Theta_1 = \Theta_2 = \Theta/2$ is chosen.

Remark. When the error in the energy norm is to be controlled then there is no need to partition the error in two parts as given in (21). Finally it leads to the desired mesh size r_τ as given in (28). The standard definitions given in the literature (see [1–3]) can be used.

6. Modeling error estimation

In general, the model is fixed in the whole domain. In this study also, an equivalent model is used, in the whole domain as the starting model. The discretization error is estimated using the patch recovery based a-posteriori error estimator and controlled by using either focussed adaptivity in the quantity of interest or global energy norm, as developed by the authors in [7,8]. Here, it is assumed

that the discretization error has been reduced significantly (with respect to modeling error). Then the total error with respect to the fixed model and the new adapted mesh is given by:

$$\|\mathbf{u}_{3D} - \mathbf{u}^{M,h}\| \approx \|\mathbf{u}_{3D} - \mathbf{u}^{M}\| \tag{29}$$

where $\|\cdot\|$ represents any desired norm. Eq. (29) assumes that the dominant part of the remaining error is due to the model. The error can be estimated using a residual type error estimator. Since a major goal of this analysis is to develop a quick but sufficiently robust estimator for the modeling error, in the following section an explicit type modeling error indicator is proposed, following Schwab [22]. The proposed modeling error indicator exploits the fact that equilibrium equations based post-processed transverse stresses are very accurate. Using these stresses gives a better representation of the actual three dimensional state of stress. Hence, the error estimator is developed using the post-processed stress state.

For a given model and its finite element approximation, the equilibrium equations based post-processed stress state (in an element) satisfies

$$\begin{aligned} &\sigma_{xx,x} + \sigma_{xy,y} + \sigma^{*}_{xz,z} = 0 \\ &\sigma_{xy,x} + \sigma_{yy,y} + \sigma^{*}_{yz,z} = 0 \\ &\sigma_{xz,x} + \sigma_{yz,y} + \sigma^{*}_{zz,z} = 0 \end{aligned} \tag{30}$$

where σ^{*}_{xz}, σ^{*}_{yz} and σ^{*}_{zz} are obtained by integration (with z) of $\sigma_{xx,x}$, $\sigma_{xy,y}$, $\sigma_{xy,x}$ and $\sigma_{yy,y}$.

Given this state of stress in an element τ, the error satisfies:

$$\left(\sigma^{ex}_{xx,x} + \sigma^{ex}_{xy,y} + \sigma^{ex}_{xz,z}\right) - \left(\sigma_{xx,x} + \sigma_{xy,y} + \sigma^{*}_{xz,z}\right) = \sigma^{er}_{xx,x} + \sigma^{er}_{xy,y} + \sigma^{er}_{xz,z} = 0 \tag{31}$$

where the superscript σ^{ex}_{ij} are the "exact" three dimensional stress components; $\sigma^{er}_{ij} = \sigma^{ex}_{ij} - \sigma^{*}_{ij}$ is the (modeling) error in the stress. Similarly, the other two equilibrium equations give

$$\begin{aligned} &\sigma^{er}_{xy,x} + \sigma^{er}_{yy,y} + \sigma^{er}_{yz,z} = 0 \\ &\sigma^{er}_{xz,x} + \sigma^{er}_{yz,y} + \sigma^{er}_{zz,z} = 0 \end{aligned} \tag{32}$$

in the interior of each element, while at the domain boundary, the error satisfies

$$\vec{T} - \vec{T}_{FE} = \vec{T}_{er} \tag{33}$$

where $\vec{T}$ is the actual applied traction vector and $\vec{T}_{FE}$ is the post-processed traction vector computed from finite element solution. In the interior of the domain an element τ has the following five interfaces:

1. Top and bottom interface (2 faces).
2. Lateral interface (3 faces).

At the top and bottom of the element interfaces the transverse stress components are continuous as the stress components are computed from equilibrium equations based post-processing. Thus, for the transverse components (on an internal interface)

$$J_i|_{\partial\tau_{transverse}} = \sigma^{\tau}_{i3} n_3 - \sigma^{\tau^*}_{i3} n_3 = 0, \quad i = 1,2,3 \tag{34}$$

where $\vec{J}|_{\partial\tau_{transverse}}$ denotes the jump vector on transverse faces. For the lateral faces

$$J_i|_{\partial\tau_{lateral}} = \sigma^{\tau}_{ij} n_j - \sigma^{\tau^*}_{ij} n_j, \quad i,j = 1,2,3 \tag{35}$$

where $\vec{J}|_{\partial\tau_{lateral}}$ denotes the jumps in the tractions at the lateral interfaces and τ^* denotes the element sharing the corresponding face of the element τ. It is observed that on all lateral faces the jumps are not zero.

It is assumed that the post-processed stresses lead to $\vec{T} - \vec{T}_{FE} = \mathbf{0}$ in the limit, that is, as the model is refined $\sum_{\partial\tau}|\vec{J}|_{L_2} \to 0$. The defined measure of modeling error $\bar{\mathbf{e}}^{M}$ can be obtained by solving (the virtual work formulations for the modeling error)

$$\begin{aligned} \mathcal{B}(\bar{\mathbf{e}}^{M}, \mathbf{v}) &= \sum_{\tau} \int_{\tau} \sigma^{er}_{ij} \varepsilon_{ij}(\mathbf{v}) dS \\ &= \sum_{\Gamma_i} \int_{\Gamma_i} \vec{J}_{\Gamma_i} \cdot \mathbf{v}\, dA + \sum_{\Gamma^k_{top} \cup \Gamma^k_{bottom}} \int_{\Gamma^k} (\vec{T} - \vec{T}^{*}) \cdot \mathbf{v} dA \end{aligned} \tag{36}$$

where $\mathbf{\Gamma}_i$ is the collection of all element faces (including those on domain boundaries) (see Fig. 4(a)). Note that on the top and bottom faces of the domain, the known state of transverse stress is used as the boundary condition for the error problem. Hence, in the elements whose transverse faces lie on the bottom domain boundary, $\vec{T} - \vec{T}_{FE} = \mathbf{0}$ (as the post-processed stress uses the known value of traction on this face as the initial value, for integration through the depth). Thus, the error problem uses the mismatch between the specified traction and the post-processed traction on the top face of the laminate only.

Eq. (36) is written as:

$$\mathcal{B}(\bar{\mathbf{e}}^{M}, \mathbf{v}) = \overline{\overline{\mathcal{F}}}(\mathbf{v}), \quad \forall \mathbf{v} \in H^0(\mathbf{V}) \tag{37}$$

where $\bar{\mathbf{e}}^{M}$ denotes the estimated modeling error. Hence, from (37),

$$\begin{aligned} \|\bar{\mathbf{e}}^{M}\|_{E(\Omega)} &= \sup_{\mathbf{v}\in H^0} \frac{|\overline{\overline{\mathcal{F}}}(\mathbf{v})|}{\|\mathbf{v}\|_{E(\Omega)}} \leqslant \sup_{\mathbf{v}\in H^0} \frac{\sum_{\Gamma_i} |\vec{J}_{\Gamma_i}|_{L_2} |\mathbf{v}|_{L_2}}{\|\mathbf{v}\|_{E(\Omega)}} \\ &\leqslant \sup_{\mathbf{v}\in H^0} \frac{\sqrt{\sum_{\Gamma i} |\mathbf{v}|^2_{L_2}} \sqrt{\sum_{\Gamma i} |\vec{J}_{\Gamma i}|^2_{L_2}}}{\|\mathbf{v}\|_{E(\Omega)}} \\ &\leqslant \sqrt{\sum_{\Gamma i} |\vec{J}_{\Gamma i}|^2_{L_2}} \sup_{\mathbf{v}\in H^0} \frac{\sqrt{\sum_{\Gamma i} |\mathbf{v}|^2_{L_2}}}{\|\mathbf{v}\|_{E(\Omega)}} \leqslant |\vec{J}|_{L_2} \sup_{\mathbf{v}\in H^0} \frac{|\mathbf{v}_{\Gamma i}|_{L_2}}{\|\mathbf{v}\|_{E(\Omega)}} \end{aligned} \tag{38}$$

where subscript $\|\cdot\|_{E(\Omega)}$ denotes the energy norm in the whole domain and L_2 denotes the L_2 norm.

This global statement can be rewritten in an elementwise form by partitioning the jumps on common faces into two parts. Several partitioning possibilities exist, but the simplest form of equal (i.e. $\alpha = \frac{1}{2}$ or half jump is assigned to each of the neighboring elements) partitioning is employed here to give

$$\|\bar{\mathbf{e}}^{M}\|_{E(\Omega)} \leqslant \sup_{\mathbf{v}\in H^0} \frac{\sum_{\tau} \left(\sum_{\partial\tau} \alpha |\vec{J}_{\partial\tau_i \cap \Gamma_i}|_{L_2} |\mathbf{v}_{\partial\tau_i \cap \Gamma_i}|_{L_2} \right)}{\|\mathbf{v}\|_{E(\Omega)}} \tag{39}$$

where $\partial\tau_i$ = faces of element τ (see Fig. 4(b)). For brevity $\partial\tau_i \cap \mathbf{\Gamma}_i$ is denoted by $\partial\tau$ in the following expressions.

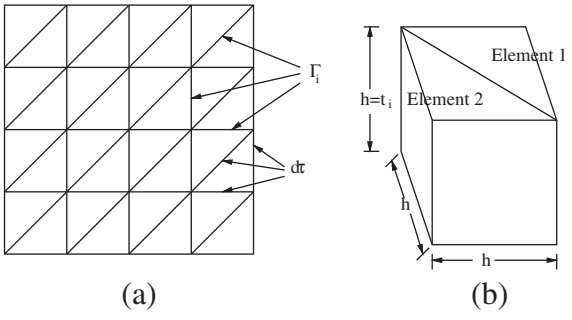

Fig. 4. (a) Mesh showing the collection of all element faces (Γ_i) and faces of an element ($\partial\tau_i$) τ; (b) types of elements used in the meshes for asymptotic behavior analysis of constant C_τ.

$$\|\bar{\mathbf{e}}^M\|_{E(\Omega)} \leqslant \frac{\sum_\tau \sum_{\partial\tau} \alpha |\vec{J}_{\partial\tau}|_{L_2} \, |\mathbf{v}_{\partial\tau}|_{L_2}}{\|\mathbf{v}\|_{E(\Omega)}} \leqslant \frac{\sum_\tau \left(\sum_{\partial\tau} \alpha^2 |\vec{J}_{\partial\tau}|^2_{L_2}\right)^{\frac{1}{2}} \left(\sum_{\partial\tau} |\mathbf{v}_{\partial\tau}|^2_{L_2}\right)^{\frac{1}{2}}}{\|\mathbf{v}\|_{E(\Omega)}} \tag{40}$$

where $\alpha = \frac{1}{2}$ for interior lateral boundaries, $\alpha = 1$ otherwise. Now

$$\sum_{\partial\tau} |\mathbf{v}_{\partial\tau}|^2_{L_2} \leqslant C_\tau \|\mathbf{v}\|^2_{E(\tau)} \tag{41}$$

where C_τ is given as

$$C_\tau = \sup_{\mathbf{v}\in H^0(\tau)} \frac{\sum_{\partial\tau} |\mathbf{v}_{\partial\tau}|^2_{L_2}}{\|\mathbf{v}\|^2_{E(\tau)}} \approx \sup_{\mathbf{v}\in H^0(\tau)} \frac{\{v\}^T [A]_{N\times N} \{v\}}{\{v\}^T [K]_{N\times N} \{v\}} \tag{42}$$

Here, **v** is chosen from a higher finite dimensional space. In this study the highest layer by layer representation corresponding to $LMp_{xy}444$ is used. Eq. (42) leads to a generalized eigenvalue problem as:

$$[A]\{v\} = \lambda [K]\{v\} \tag{43}$$

The generalized eigenvalue problem is solved once and the constant C_τ is found as $C_\tau = \lambda_{max}$.

From (40)

$$\|\bar{\mathbf{e}}^M\|_{E(\Omega)} \|\mathbf{v}\|_{E(\Omega)} \leqslant \sum_\tau \left(C_\tau \|\mathbf{v}\|^2_{E(\tau)}\right)^{\frac{1}{2}} \left(\sum_{\partial\tau} \alpha^2 |\vec{J}_{\partial\tau}|^2_{L_2}\right)^{\frac{1}{2}} \leqslant \sum_\tau (\|\mathbf{v}\|^2_{E(\tau)})^{\frac{1}{2}} C_\tau^{\frac{1}{2}} \left(\sum_{\partial\tau} \alpha^2 |\vec{J}_{\partial\tau}|^2_{L_2}\right)^{\frac{1}{2}} \tag{44}$$

that is

$$\|\bar{\mathbf{e}}^M\|_{E(\Omega)} \leqslant \sum_\tau \left(C_\tau \sum_{\partial\tau} \alpha^2 |\vec{J}_{\partial\tau}|^2_{L_2}\right)^{\frac{1}{2}} \tag{45}$$

The element (modeling error) indicator is defined as

$$\eta^M_\tau = (C_\tau)^{\frac{1}{2}} \left(\sum_{\partial\tau} \alpha^2 |\vec{J}_{\partial\tau}|^2_{L_2}\right)^{\frac{1}{2}} \tag{46}$$

and global estimated modeling error as

$$\|\bar{\mathbf{e}}^M\|^2_{E(\Omega)} = \sum_\tau (\eta^M_\tau)^2 \tag{47}$$

Note that the estimator is an upper estimator, with the global effectivity index given as

$$\kappa^M_\omega = \frac{\|\bar{\mathbf{e}}^M\|_{E(\Omega)}}{\|\mathbf{e}^M\|_{E(\Omega)}} \tag{48}$$

where $\|\mathbf{e}^M\|_{E(\Omega)}$ is exact modeling error over the whole domain. The modeling error tolerance achieved is given as

$$\Theta_M = \frac{\|\bar{\mathbf{e}}^M\|_{E(\Omega)}}{\sqrt{2\mathcal{U}(\mathbf{u})}} \tag{49}$$

where $\mathcal{U}(\mathbf{u})$ is strain energy for the given plate model.

Note that the eigenvalue problem can be written only in terms of the **v** defined on the element's lateral faces as:

$$[A_{SS}]\{v_S\} = \lambda [\overline{K}]\{v_S\} \tag{50}$$

where $[\overline{K}] = -[K_{IS}]^T [K_{II}]^{-1} [K_{IS}] + [K_{SS}]$. Here, $[A_{SS}]$ is symmetric positive definite and $[\overline{K}]$ is symmetric positive semi-definite. Here, subscript I corresponds to internal degrees of freedom and S corresponds to surface degrees of freedom of the element.

In the above generalized eigenvalue system the first six modes correspond to the rigid modes. These can be eliminated to further reduce the size of the matrices. The first non zero eigenvalue gives the constant C_τ. The details of this can be seen in [10,22].

Remark. The calculation of exact stresses is not required in the proposed approach. The inter-element jumps in the stresses across the element faces are calculated for the model that is used in the analysis. The equilibrium equations based post-processing is used to obtain the transverse stresses. These stresses are taken as exact stresses. These stresses are used to calculate the inter-element jumps across the element faces.

Remark. For calculating the global effectivity index, as in (48), one needs to have the exact solution. However, this is not possible for all the problems. Hence, in general, a sufficiently refined mesh (with element size of the order of lamina thickness) and enriched model (in the present case LM4444) is used as the "exact solution". Using this exact solution, $\|\mathbf{e}^M\|_{E(\Omega)}$ is calculated in (48). This is done only for benchmarking problems to show the reliability of the proposed modeling error indicator.

7. Modeling error control

Modeling error is controlled by locally using higher models in regions of high modeling error. The initial model used for the analysis is an equivalent model $EQp_{xy}p^z_u p^z_v p^z_w$, written as EQ for brevity. The steps followed in the modeling error control methodology are given as follows.

Step 1: The element indicator η^M_τ, for each element τ is computed as given in (46).

Step 2: Maximum value of element indicator from all elements $(\eta^M_{\tau_{max}})$ is found.

Step 3: All the element modeling error indicators are normalized as:

$$A_\tau = \frac{\eta^M_\tau}{\eta^M_{\tau_{max}}}$$

Step 4: As a rule of thumb, the set of $3D$ elements (here denoted as τ) with $A_\tau \geqslant 0.5$ is found. The set of projection of these elements on the planar mesh (denoted by $A_{\tau_{2D}}$) is then found.

The strategy for adapting the models is explained as follows.

In the regions with $2D$ elements $\tau_{2D} \subseteq A_{\tau_{2D}}$ corresponding $LMp_{xy}p^z_u p^z_v p^z_w$, written as LM for brevity, model is adopted. The problem is solved again with these new regionwise models in the domain and the modeling error tolerance achieved is checked for. If the tolerance achieved is below the specified tolerance then steps 1–4 are repeated. Then new set $A_{\tau_{2D}}$ is found. If the new set $A_{\tau_{2D}}$ has elements other than those in the old set then the region corresponding to these elements are made layerwise. If the same $3D$ element is again in the set with $A_\tau \geqslant 0.5$, then the layer corresponding to this element is subdivided into two layers (sublayers) locally. This process is continued till the specified modeling error tolerance is achieved.

Remark. In the design of aerospace laminated structural components the effects of boundary layer, edge and loading constraints, local delaminations, free edges, damage fronts, re-entrant corners, cut-outs, etc. are very important from design point of view. The quantities like stress state, stress concentrations, displacement components, etc. are the critical quantities for such design considerations. If the errors in the discretization and modeling

are not controlled with the use of proper mesh and model, then it can lead to erroneous results in these critical quantities. However, in the present approach selection of proper mesh and model is done automatically ensuring that the discretization and modeling error are within acceptable limits leading to accurate computation of critical quantities. Thus, mesh and model sensitivity is automatically accounted for, leading to higher reliability of computations.

8. Numerical results

We now present detailed results. The numerical results demonstrate the accuracy of various plate models and quality of the discretization and modeling error estimators. Examples with mesh and model adaptivity are also given.

8.1. Global quality of a-posteriori discretization error estimator

The global quality of a-posteriori error estimator is tested for two different plate to thickness ratios of $S = \frac{a}{t}$ (a is length and t is thickness of laminate) 50, 100; and boundary conditions of all edges clamped (CCCC) and hard simple supported (HSSSS). The material is *M*55*J*/*M*18 and its properties are given in Table 1. The laminates considered are [0/90] and [45/−45] under uniform transverse load of 1 N/mm^2. Here, *EQ*2332 and *LM*2332 models are considered. The global effectivity index for the laminates considered are given in Tables 2 and 3 for *EQ*2332 and *LM*2332 models, respectively. The mesh used for this study is shown in Fig. 5(a). From these tables it is seen that the estimator is reliable for all the laminates considered ($1.06 \leqslant \kappa_\omega \leqslant 1.35$).

Note that in the global behavior the effect of boundary conditions and plate length to thickness ratio is minimal. However, from [6], it can be seen that the local quality can be different for boundary patches, as compared to internal ones.

8.2. Comparison of plate models

In this subsection, *EQ*, *LM* and *RR* plate models are compared for stress state and displacement at a point. A nine layered [0/90/0/90/0/90/0/90/0] laminate, with all edges hard simple supported and with material properties given in Table 4 (see [43]), is considered. The thickness of each 0° layer is 1 *in*; thickness of each 90° layer is 1.25 in. The laminate has dimensions of $a = b = 100$ in. The laminate is subjected to sinusoidal loading of the form $T_3(x,y) = q_0 \sin\frac{\pi x}{a} \sin\frac{\pi y}{b}$ where q_0 is the intensity of sinusoidal loading. The stress components are normalized as $\bar{\sigma}_{xx} = \frac{1}{q_0 S^2}\sigma_{xx}$ and $\bar{\tau}_{xz} = \frac{1}{q_0 S}\tau_{xz}$, displacement component u is normalized as $\bar{u} = \frac{E_{22} u}{q_0 S^3}$. The objective is to obtain the values of $\bar{\sigma}_{xx}$ at $(\frac{a}{2}, \frac{b}{2}, \bar{z})$, $\bar{\tau}_{xz}$ at $(0, \frac{b}{2}, \bar{z})$, as shown in Fig. 6(a) and (b), accurately. For this purpose, the *LM*3332 and *EQ*3332 models have been used. Further, region-by-region modeling scheme is also used with model distribution as shown in Fig. 7(a) and (b). For the region-by-region modeling scheme, in the shaded region (which is a neighborhood of the point of interest) *LM*3332 model is used, while in the remaining regions *EQ*3332 model is used. The region-by-region modeling scheme used for stress components $\bar{\sigma}_{xx}$ is denoted by *RR I* − 3332 and for $\bar{\tau}_{xz}$ by *RR II* − 3332. The variation of $\bar{\tau}_{xz}$ at $(0, \frac{b}{2}, \bar{z})$, obtained by using the equilibrium equations based post-processing, is given in Fig. 6(c). The respective stress components in Fig. 6(a)–(c) are compared with exact three dimensional elasticity solution obtained by Pagano et al. in [43] and is denoted by "Pagano" in these figures. The pointwise value of displacement component $\bar{u}$ at $(0, \frac{b}{2}, \bar{z})$ is given in Fig. 8. This figure also shows the displacement component obtained by exact three dimensional elasticity solution obtained by Pagano et al. [43] and is denoted by "Pagano" in this figure. The number of unknowns and strain energy for these modeling schemes is given in Table 5.

From the figures and table it is seen that:

1. The discretization error, for the given mesh and for all the models, is below the specified tolerance (here, $\Theta = |\mathcal{F}(\mathbf{e}^{M,*})|/|\mathcal{F}(\mathbf{e}^{M,h})| = 2\%$ is specified). Here, the discretization error in the energy norm is controlled.
2. The in-plane stress component $\bar{\sigma}_{xx}$ is accurately computed by all the models.
3. The transverse stress component directly computed from finite element data is very accurate for *LM*3332 and *RR II* − 3332 model (it almost overlaps the exact one) while for *EQ*3332 model it is very far both qualitatively and quantitatively.
4. The equilibrium equations based post-processing approach is accurate for all models. The accuracy of the post-processed stress components depends upon the accuracy of in-plane stresses used.
5. The cost of computation for *LM*3332 model is very high while for the *EQ*3332 model the cost is low. Notably, the cost of computation for *RR I* − 3332 and *RR II* − 3332 models is close to that for the *EQ*3332 model and is significantly lower than the *LM*3332 model.
6. Note that the value of strain energy obtained by using the given models varies as $\mathcal{U}_{EQ3332} < \mathcal{U}_{RRI-3332} < \mathcal{U}_{RRII-3332} < \mathcal{U}_{LM3332}$.

Table 2
Global quality (κ_ω) of discretization error estimator for *EQ*2332 model, *M*55*J*/*M*18 material.

Laminate	*S*	BC	κ_ω
[0/90]	50	SSSS	1.0594
		CCCC	1.1725
	100	SSSS	1.1337
		CCCC	1.2858
[45/−45]	50	SSSS	1.1379
		CCCC	1.2283
	100	SSSS	1.2173
		CCCC	1.3396

Table 3
Global quality (κ_ω) of discretization error estimator for *LM*2332 model, *M*55*J*/*M*18 material.

Laminate	*S*	BC	κ_ω
[0/90]	50	SSSS	1.0635
		CCCC	1.1792
	100	SSSS	1.1427
		CCCC	1.3021
[45/−45]	50	SSSS	1.1428
		CCCC	1.2368
	100	SSSS	1.2311
		CCCC	1.3585

Table 1
Material properties for *M*55*J*/*M*18 and *T*300/5208 Graphite/Epoxy composite.

Property	E_{11} (GPa)	$E_{22} = E_{33}$ (GPa)	$G_{12} = G_{13} = G_{23}$ (GPa)	$\nu_{12} = \nu_{13} = \nu_{23}$	t_i (mm)
*M*55*J*/*M*18	280	6.0	4.8	0.3	0.1
*T*300/5208	132.5	10.8	5.7	0.24	0.127

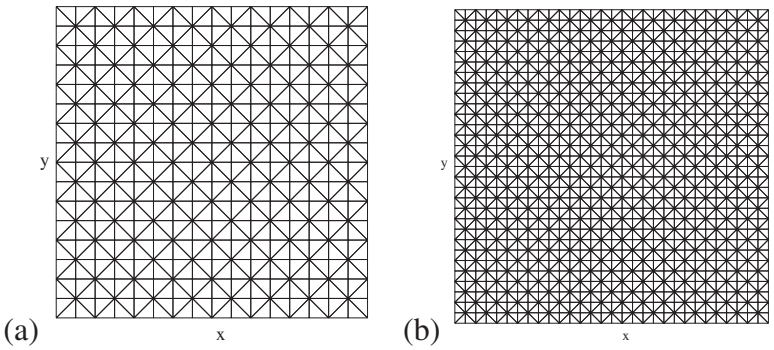

Fig. 5. Mesh used for the (a) study of global quality of a-posteriori discretization error estimator and (b) study of global quality of modeling error estimator.

Table 4
Material properties for Graphite/Epoxy composite [43].

Property	E_{11}	$E_{22} = E_{33}$	$G_{12} = G_{13} = G_{23}$	$\nu_{12} = \nu_{13} = \nu_{23}$
Value	25×10^6 psi	10^6 psi	0.5×10^6 psi	0.3

The current example also illustrates a few very important issues. These are:

(a) Even though the *RRI* – 3332 and *RRII* – 3332 models give very accurate values of the local stress and displacements, in the region of interest, the overall accuracy (with respect to global strain energy) is low. This is because outside the region of interest, a low order equivalent model has been used.
(b) Often (especially for thin, symmetric laminates) the equivalent models are very effective, provided the equilibrium equations based post-processing is used to obtain the transverse stresses. This makes the equivalent models, which are easier to implement, attractive.

8.3. Global quality of the modeling error estimator

The global error estimator, as defined by (48), requires computation of the constant C_τ. The constant depends on the geometry of the elements and the mesh size. Since the modeling error estimate is obtained for the mesh for which the discretization error is negligible, the corresponding converged mesh will have sufficiently small elements. Hence, it is necessary to obtain the value of C_τ for such a mesh. Below, we investigate the behavior of this constant, with respect to mesh-size and element geometry.

Remark. In all the numerical examples for the modeling error estimator, all the energy quantities are computed using equilibrium equations based post-processed transverse stresses. Thus, the strain energy computed becomes the complementary strain energy.

8.3.1. Asymptotic behavior of constant C_τ

The asymptotic behavior of constant C_τ is studied for *M*55J/*M*18 and *T*300/5208 Graphite/Epoxy materials. The starting model used is *EQ*3333 and the highest model used is *LM*3444. The two types of element geometries used in this study are given in Fig. 4(b). The size of the element is taken as a multiple of the layer thickness, and is given by $h = \alpha t$. Here, α is a scalar variable. The variation of C_τ with α is shown in Fig. 9(a) and (b). The effect of mesh topology is also depicted in these figures. From these figures it is seen that:

1. The value of C_τ converges to that for $\alpha = 1$, i.e. $h \to t_i$.
2. For the geometry of Element 1, the variation of C_τ with mesh size is significant, while the change for Element 2 is small.

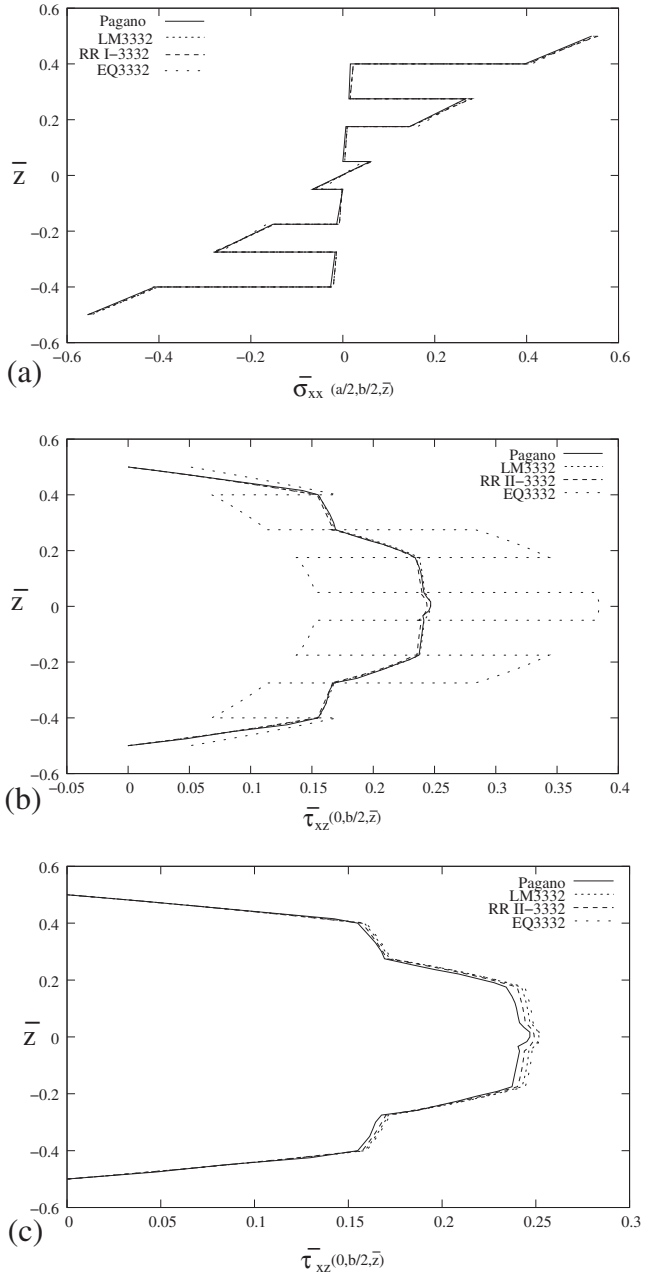

Fig. 6. Comparison of through thickness variation of stresses in [0/90/0/90/0/90/0/90/0] laminate; $S = 10$; under sinusoidal loading with all edges hard supported. (a) In-plane stress $(\bar{\sigma}_{xx}(\frac{a}{2}, \frac{b}{2}, \bar{z}))$; (b) direct transverse shear stress $(\bar{\tau}_{xz}(0, \frac{b}{2}, \bar{z}))$; (c) post-processed transverse shear stress $(\bar{\tau}_{xz}(0, \frac{b}{2}, \bar{z}))$.

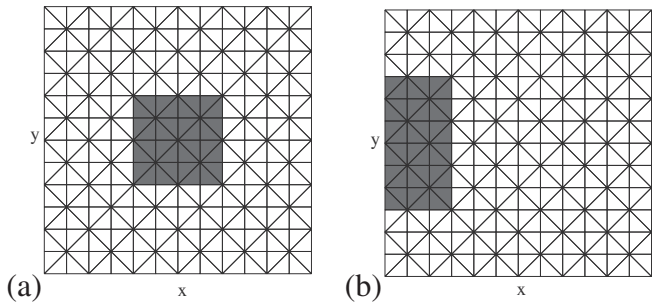

Fig. 7. Region-by-region schemes used for the computation of stress components $\bar{\sigma}_{xx}(\frac{a}{2},\frac{b}{2},\bar{z})$ and $\bar{\tau}_{xz}(0,\frac{b}{2},\bar{z})$ for [0/90/0/90/0/90/0/90/0] laminate; $S = 10$; under sinusoidal loading with all edges hard supported. Shaded region shows *LM*3332 model and rest uses *EQ*3332 model. (a) *RRI* – 3332 model and (b) *RRII* – 3332 model.

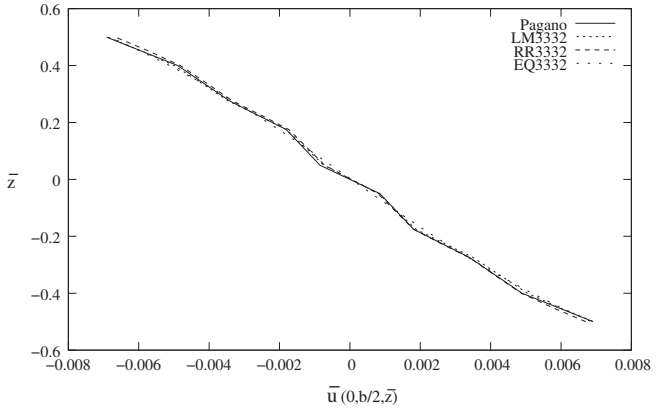

Fig. 8. Through thickness variation of in-plane displacement $\bar{u}$ for [0/90/0/90/0/90/0/90/0] laminate; $S = 10$; under sinusoidal loading with all edges hard supported.

Table 5
Comparison of plate models on the basis of displacement and stress components for [0/90/0/90/0/90/0/90/0] square laminate; $S = 10$ with all edges hard simple supported under sinusoidal loading. The number of unknowns and strain energy are given.

Model	Unknowns	$2\mathcal{U}$
*LM*3332	102,675	0.8161
RR I − 3332	22,803	0.7640
RR II − 3332	24,851	0.7732
*EQ*3332	15,059	0.7628

3. For both element types, the converged value of C_τ is the same. For *M*55*J*/*M*18 material this value is 115.38×10^{-6}.

The effect of ply orientation, on the converged value of C_τ, was also studied by authors [10]. It was observed that the variation was not significant. Hence, the value obtained for ply orientation of $\theta = 0^\circ$ has been used in all studies.

Remark. For a given material the converged value of C_τ, corresponding to $h = t_i$, is used for all mesh sizes. Hence, when the material is different for different laminae in a laminate or within a lamina (as in case of damaged lamina) the value of C_τ is computed for individual material regions.

Remark. For the computations, asymptotic value of the constant C_τ is used. In order to determine C_τ, the eigenvalue problem is first solved over a unit triangular element with length and thickness taken as one (as shown in Fig. 4(b)). Let the value of constant obtained be $\widehat{C}$. The value of C_τ for an element with edges of size $h = t_i$ (where t_i is the thickness) is obtained as $C_\tau = \widehat{C} t_i$.

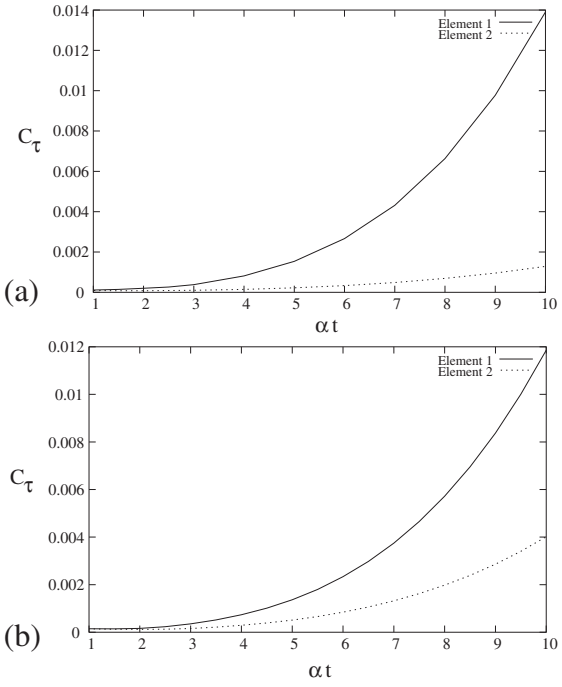

Fig. 9. Asymptotic behavior of constant C_τ with respect to mesh size (t is thickness of the element τ) for material (a) *M*55*J*/*M*18; (b) *T*300/5208.

8.3.2. Quality of the modeling error estimator

The global quality of the proposed modeling error estimator is obtained by computing the effectivity index for two values of length to thickness ratios, *S*. The effectivity index for length to thickness ratios of 50, 100 and two boundary conditions either all edges clamped or hard simple supported are computed for *M*55*J*/*M*18 Graphite/Epoxy material. The laminate is subjected to uniform transverse load of intensity $T_3(x,y) = 0.025$ N/mm^2. The mesh used for this study is given in Fig. 5(b). This mesh corresponds to small discretization error in energy norm ($\Theta < 1\%$). The model considered for this study is *EQ*3222. The highest model considered is *LM*3222. Note that the solution for *LM*4444 is used as the "exact" solution, in all the computations of modeling error.

The global effectivity indices for [0/90] and [45/−45] laminates are given in Tables 6 and 7, respectively. Further, the values of the estimated and (representative) "exact" modeling error, along with the energy of the finite element solution ($\|\mathbf{u}^{EQ,h}\|_{E(\Omega)}$ and $\|\mathbf{u}^{LM,h}\|_{E(\Omega)}$) are also reported. From these tables it is seen that:

1. The proposed modeling error estimator is an upper estimator, as has been proven in (45).
2. For both the cross-ply and angle-ply laminates, the estimator is good for the HSSSS boundary conditions, while for the CCCC boundary condition, the overestimation can be high ($\kappa_\omega^M \approx 5$).
3. As the mesh size approaches the thickness of a lamina ($t_i = 0.1$ mm) the quality of estimator improves (approaches the value of 1). This can be seen from the values of effectivity index for $S = 50$, 100. For $S = 50$ the mesh size is $h = 0.33$ mm while for $S = 100$, $h = 0.66$ mm.
4. The relative (estimated) modeling error $\left(\sqrt{\frac{\|\mathbf{e}^M\|^2_{E(\Omega)}}{\|\mathbf{u}^{EQ,h}\|^2_{E(\Omega)}}}\right)$ is small in most cases ($\leqslant 6\%$) except for [45/−45] laminate with $S = 50$ and all edges hard simple supported (25.5%).

This example brings out the important issue of plate boundary conditions for polygonal domains. This issue is elucidated with

Table 6
Global quality (κ_{ω}^{M}) of modeling error estimator; [0/90] laminate under uniform transverse load of intensity $T_3(x,y) = 0.025$ N/mm^2 for *M55J/M18* material. Norms are computed using post-processed stresses. Mesh is shown in Fig. 5(b).

BC	S	$\|\bar{\mathbf{e}}^M\|^2_{E(\Omega)}$	$\|\mathbf{e}^M\|^2_{E(\Omega)}$	$\|\mathbf{u}^{EQ,h}\|^2_{E(\Omega)}$	$\|\mathbf{u}^{LM,h}\|^2_{E(\Omega)}$	(κ_{Ω}^{M})	Θ%
CCCC	50	1.74×10^{-5}	3.83×10^{-6}	5.05×10^{-3}	5.05×10^{-3}	2.13	0.010
	100	6.34×10^{-4}	2.95×10^{-5}	3.13×10^{-1}	3.13×10^{-1}	4.63	0.013
HSSSS	50	3.24×10^{-7}	2.61×10^{-7}	2.92×10^{-2}	2.92×10^{-2}	1.12	8.35×10^{-6}
	100	1.67×10^{-5}	1.59×10^{-5}	1.86	1.86	1.03	2.54×10^{-5}

Table 7
Global quality (κ_{ω}^{M}) of modeling error estimator; [45/−45] laminate under uniform transverse load of intensity $T_3(x,y) = 0.025$ N/mm^2 for *M55J/M18* material. Norms are computed using post-processed stresses. Mesh is shown in Fig. 5(b).

BC	S	$\|\bar{\mathbf{e}}^M\|^2_{E(\Omega)}$	$\|\mathbf{e}^M\|^2_{E(\Omega)}$	$\|\mathbf{u}^{EQ,h}\|^2_{E(\Omega)}$	$\|\mathbf{u}^{LM,h}\|^2_{E(\Omega)}$	(κ_{Ω}^{M})	Θ%
CCCC	50	1.68×10^{-5}	2.57×10^{-6}	5.62×10^{-3}	5.62×10^{-3}	2.55	0.013
	100	4.66×10^{-4}	1.84×10^{-5}	3.47×10^{-1}	3.47×10^{-1}	5.03	0.014
HSSSS	50	9.76×10^{-4}	9.12×10^{-5}	1.08×10^{-2}	1.09×10^{-2}	3.27	0.105
	100	2.91×10^{-2}	1.55×10^{-3}	6.75×10^{-1}	6.75×10^{-1}	4.33	0.105

following example. For thick plate ([45/−45] laminate with $S = 5$), behavior of effectivity index with mesh size for clamped and hard supported boundary conditions is shown in Table 8. The meshes used are shown in Fig. 10. As the mesh size approaches the lamina thickness the effectivity index tends to the value of 1. However, this is not observed for the case of hard simple supported laminate. This is because for hard simple support, the plate paradox plays a dominant role in the three dimensional models, along with the Kirchhoff model (see [44] for more details) and hierarchic plate models (see [45] for more details). It is shown, [45], that in a paradoxical behavior of the hard simple support the difference between hard and soft support need not necessarily be constrained to a small neighborhood of the boundary, but can influence the solution in the entire domain (see [44]). A detailed study on this behavior of homogeneous square plates under uniform load can be seen in [46]. In case of angle-ply laminates, this behavior can be significant. This can be seen through the distribution of the norm of the interelement jumps shown for each lamina in Fig. 11(a) and (b) for all edges hard simple supported and in Fig. 11(c) and (d) for all edges clamped for Mesh 4 used in this study. The norms are scaled by the maximum value of the norm (which is 6.94×10^{-5} for all edges hard supported and 8.18×10^{-7} for all edges clamped). It is to be noted that value of the norm is more at the corners of -45° lamina. Also note that the ratio of the highest value of the error for these two boundary conditions is approximately 100. This points to the effect of the plate paradox situation, as well as unsmoothness of solution in the corners for hard simple support case. At other places the value of the norm is very low compared to the value at the corners. For Mesh 4 the norm of the jumps are recomputed with one layer of elements on all the boundaries excluded and referred to as Mesh 4* in Table 8. It can be seen that the estimated norm of the modeling error is reduced and effectivity index is improved to 1.49. The maximum value of the norm for this case is 6.04×10^{-7}. In this example if the elements at the corners of -45° lamina are excluded, the norm of the jump will reduce, leading to improved effectivity index.

The value of the norm of the jumps depends upon the constant C_{τ} and the interelement jumps. The value of the constant at constrained boundaries is different from the other elements and is lower. However, in this analysis this aspect is not implemented and all the elements have same constant C_{τ}. This makes the value of the norm higher at the constraint boundaries than they are. Also, the interelement jumps do not reduce even with mesh refinements in the case of hard support. These two factors increase the norm of the jump leading to increased effectivity index. A graded mesh refinement in the plate corners will lead to reduction in jump values. This is motivated by the work done by Babuška and Scapolla [47] on performance evaluation for a rhombic plate bending problem. The size of the elements in the corner, for which the jumps are very high, is reduced. This leads to a smaller values of jumps in the corner. This is shown in Table 8 for the Mesh 5 (mesh given in Fig. 10). The graded refinement along all the boundaries would also have given similar results.

Hence, the proposed modeling error estimator accurately captures the plate paradox for hard simple support.

Table 8
Global quality (κ_{ω}^{M}) of modeling error estimator; [45/−45] laminate under uniform transverse load of intensity $T_3(x,y) = 0.025$ N/mm^2 for *M55J/M18* material; $S = 5$. See Fig. 10 for meshes used in this study.

BC	Mesh	$\|\bar{\mathbf{e}}^M\|^2_{E(\Omega)}$	$\|\mathbf{e}^M\|^2_{E(\Omega)}$	$\|\mathbf{u}^{EQ,h}\|^2_{E(\Omega)}$	$\|\mathbf{u}^{LM,h}\|^2_{E(\Omega)}$	(κ_{Ω}^{M})	Θ%
CCCC	Mesh 1	3.31×10^{-8}	7.84×10^{-10}	2.63×10^{-8}	2.56×10^{-8}	6.49	9.178
	Mesh 2	1.14×10^{-8}	1.37×10^{-9}	2.66×10^{-8}	2.57×10^{-8}	2.89	0.677
	Mesh 3	4.93×10^{-9}	1.66×10^{-9}	2.64×10^{-8}	2.54×10^{-8}	1.72	0.163
	Mesh 4	2.72×10^{-9}	1.81×10^{-9}	2.63×10^{-8}	2.52×10^{-8}	1.22	0.064
HSSSS	Mesh 1	4.64×10^{-8}	1.22×10^{-9}	3.21×10^{-8}	3.25×10^{-8}	6.17	10.52
	Mesh 2	4.69×10^{-8}	1.46×10^{-9}	3.37×10^{-8}	3.38×10^{-8}	5.66	1.32
	Mesh 3	6.59×10^{-8}	1.67×10^{-9}	3.46×10^{-8}	3.43×10^{-8}	6.28	0.06
	Mesh 4	9.58×10^{-8}	1.84×10^{-9}	3.55×10^{-8}	3.49×10^{-8}	7.21	0.05
	Mesh 4*	4.10×10^{-9}	1.84×10^{-9}	3.55×10^{-8}	3.49×10^{-8}	1.49	0.05
	Mesh 5	2.01×10^{-7}	2.77×10^{-8}	3.48×10^{-8}	3.48×10^{-8}	2.69	0.01

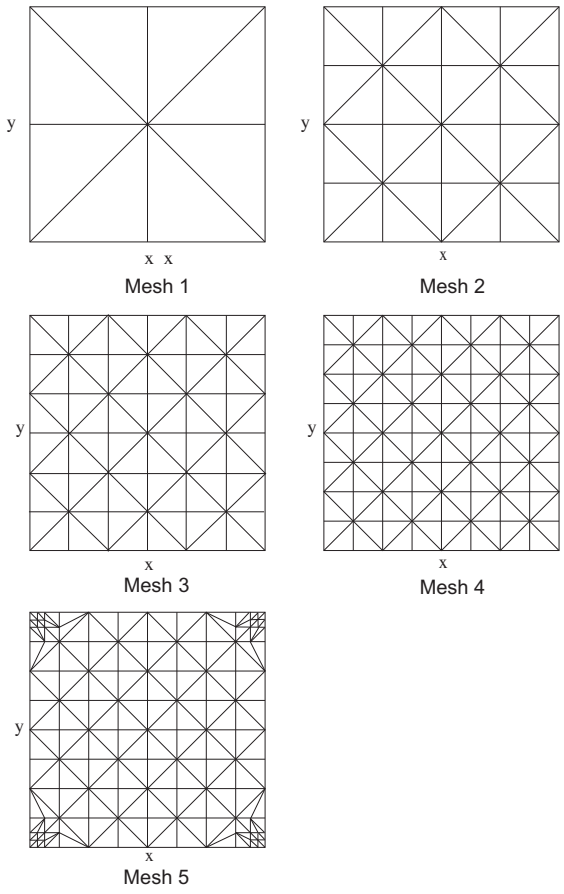

Fig. 10. Meshes used for the study of behavior of modeling error effectivity index.

8.4. Domain with static damage

In this section two numerical examples with modeling error estimation and control are presented.

Here, the laminate stacking sequence, geometry, boundary conditions and material properties are same as given in Section 8.2. However, the load is uniformly distributed over the top surface with $T_3(x,y) = 1$ lb/in.^{2}. The initial model used is $EQ3332$ in the whole domain. The specified tolerance for discretization error is 1%. The initial mesh used is shown in Fig. 12(a). In this example, three types of static damages, of fixed size of 16.67×16.67 in., are considered. The planar location of these damages in the domain are shown in Fig. 12(b).

The damage in a lamina is incorporated using "damage meso-model" as proposed by Ladevèze et al. in [34]. This is a continuum based damage model. The effect of the damage is manifested by degradation of material properties through damage indicators or parameters. The key feature of this model is that it has a separate indicator for each damage mechanisms in ply and interface. Further, it clearly differentiates the behavior under "tensile" and "compressive" stress states. For transversely isotropic laminae the effect of damage is modeled as follows.

The effect of damage in normal modes is modeled as

$$E_1^d = \begin{cases} E_1(1-d_1) & \text{if } \sigma_{11} \geqslant 0 \\ 0 & \text{if } \sigma_{11} < 0 \end{cases} \text{ and } E_2^d = \begin{cases} E_2(1-d_2) & \text{if } \sigma_{22} \geqslant 0 \\ 0 & \text{if } \sigma_{22} < 0 \end{cases} \tag{51}$$

and in shear modes as

$$G_{12}^d = G_{12}(1-d_3) \text{ and } G_{23}^d = G_{23}(1-d_4) \tag{52}$$

with

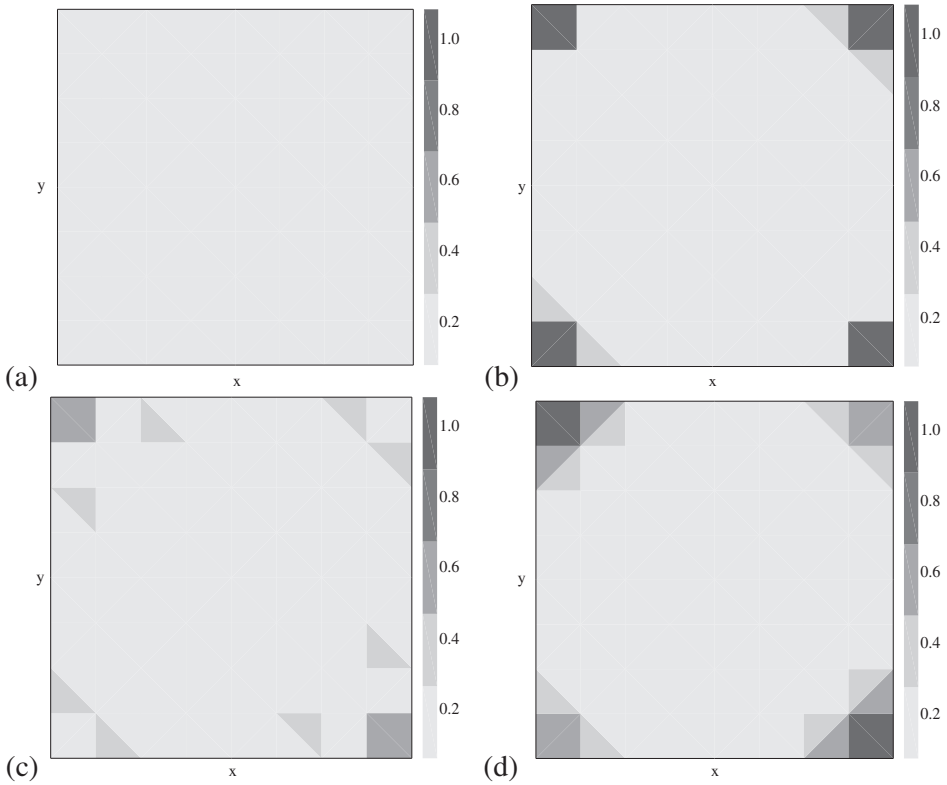

Fig. 11. Distribution of the norm of the interelement jumps in lamina for (a) 45°; (b) −45° lamina with hard simple support and for (c) 45°; (d) −45° lamina with clamped boundary conditions for Mesh 4 in Fig. 10.

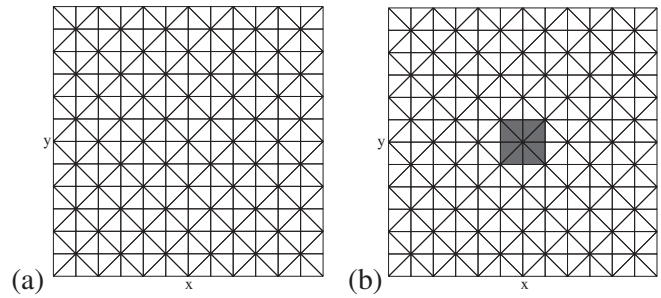

Fig. 12. Discretization and modeling error control in domain with static damage in [0/90/0/90/0/90/0/90/0] laminate; $S = 10$; under uniform transverse loading of intensity $T_3(x,y) = 1$ N/mm^2. (a) Initial mesh; (b) location and size of static damage.

$$\frac{v_{ij}^d}{E_{ij}^d} = \frac{v_{ij}}{E_{ij}} \tag{53}$$

where the superscript d stands for "damaged", d_1, d_2, d_3 and d_4 are the damage indicators for fiber-break, matrix normal crack, interface shear crack damage modes, respectively. The other quantities have their standard meanings as in laminated composites. For interface, the effect of damage on the interface material is given as

$$E^d = E(1 - d_5) \tag{54}$$

where E is Young's modulus of the interface material and d_5 is the delamination damage indicator. It is assumed that the intensity of damage is same in all three modes of delamination. For more details of this model for ply damage mechanisms refer to [35,36] and references therein. For interface damage (delamination) model refer to [37–39] and references therein.

In the following examples, only static damage cases are implemented and no attempt has been made to study the propagation of damage. For more details on this see the work done by authors in [10].

8.4.1. Matrix cracking damage ($d_2 > 0$)

The bottom-most 90° layer has a matrix cracking damage. In this example it is assumed that the matrix damage causes the degradation of E_2 by 80% in the region shown in Fig. 12(b). Thus, in this region $E_2^d = 0.2E_2$ is taken. The discretization error for the initial mesh with *EQ*3332 model and modeling error are very low. The error indicators predict that there is no need for mesh and model adaptivity. The scaled modeling error energy density distribution in this layer is shown in Fig. 13. This is expected, as matrix cracking has a weak influence on overall response.

8.4.2. Delamination ($d_5 > 0$)

The fifth interface between 0° and 90° layers from the top of the laminate has delamination. This interface has been assumed as a thin layer of epoxy material (see Table 9 for properties). Here, Young's modulus of epoxy material is degraded by 80% in the delaminated area. The predicted discretization and modeling error are very low for this mesh and *EQ*3332 model. Hence, mesh and model adaptivity is not needed. The scaled modeling error energy density distribution in this layer is shown in Fig. 14.

8.4.3. Fiber damage ($d_1 > 0$)

The top-most 90° layer has broken fibers in the damaged region. In this region, $E_1^d = 0.2E_1$ is taken. The discretization error for this mesh with initial model *EQ*3332 is within a specified tolerance of 1%. This mesh is then fixed and model adaptivity is carried out. The scaled modeling error energy distributions is shown in Fig. 15 while the model distribution in the domain are shown in Figs. 16 and 17. The modeling error for the initial mesh and *EQ*3332 model is 64.58%. The scaled error energy density distribution in this layer is shown in Fig. 15(a). In the second step, *LM*3332 model is adapted in the shaded region as shown in Fig. 16(a). The modeling error for this model is 33.93%. The scaled error energy density distribution in this layer is shown in Fig. 15(b). In the third step, more region is made as layerwise as shown by shaded region in Fig. 16(b). The layers 7 and 8 are further divided into two sublayers each (see Fig. 17(a)). The modeling error for this model is 25.04%. The scaled error energy density distribution in the sublayers of layer 8 is shown in Fig. 15 (c) and (d). Finally, all the bottom six original layers are divided into two sublayers each and sublayers of original eighth layer are further divided into two sublayers each (see Fig. 17(b)). Thus, there are 19 layers (including sublayers) in this model with layerwise region shown in the Fig. 16(c). The scaled error energy density distribution for the top-most sublayer of the original eighth layer is shown in Fig. 15(e), while for other layers the scaled density of energy of the error is very low. The modeling error for this model is 17.82%.

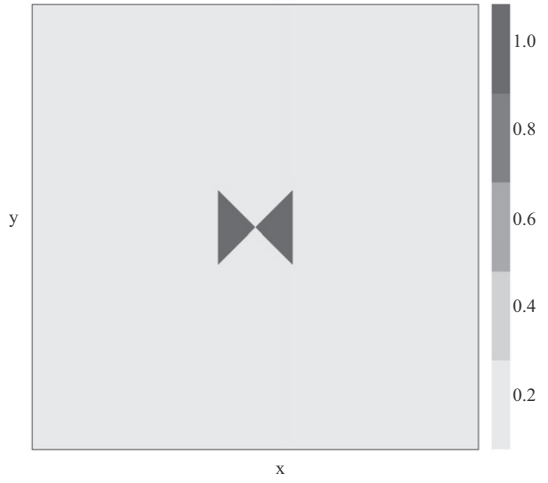

Fig. 13. Distribution of scaled modeling error energy for matrix cracking damage.

From this study it can be observed that:

1. The discretization error for *EQ*3332 model with initial mesh for all damage cases is achieved within specified tolerance with discretization error control in energy. For matrix cracking and delamination damage the discretization error is very low compared to that with fiber breakage damage.
2. The effect of matrix cracking and delamination damage do not have significant effect on modeling error. The *EQ*3332 model with discretization error controlled is sufficient for modeling error to be within acceptable limit.
3. Fiber breakage damage has significant effect on modeling error. The modeling error is maximum at the damage front in the fiber direction.
4. The use of sublayers in the fiber damaged layers is very effective in controlling the modeling error.
5. The values of strain energy, given in Table 10, using equilibrium equations based post-processed transverse stresses. These values show convergence from above as this energy is complementary to strain energy.

Table 9
Material properties for Epoxy.

Property	$E_{11} = E_{22} = E_{33}$	$v_{12} = v_{13} = v_{23}$
Value	0.67×10^6 psi	0.38

Fig. 14. Distribution of scaled modeling error energy for delamination damage.

8.4.4. Comparison with Abaqus/Standard

In this study a [0/90/0] laminate of $a = b = 30$ mm with each layer of thickness 0.1 mm and material properties for *M*55*J*/*M*18 as given in Table 1 with fiber damage of size 7.5 mm × 7.5 mm in 90° ply at the center of the plate, as shown in Fig. 18(a) is considered. The Young's modulus of the damaged region is given by $E_1^d = 0.2E_1$, where E_1 is the modulus for healthy region. The initial mesh used for the analysis is shown in Fig. 18(a). The laminate is soft simple supported on all edges and subjected to transverse uniform load of 1 N/mm^2 on top face. Initially *EQ*2222 model is used everywhere in the domain. The discretization error for this mesh and model is 6.67%. The discretization error is controlled to 0.55%. This value is below the specified discretization error tolerance of 1%. The final mesh (along with the fiber damage zone) is shown in Fig. 18(b). With this mesh and laminate model *EQ*2222, the modeling error tolerance achieved is 5.3%. This indicates that the model *EQ*2222 is not sufficient to achieve the specified modeling error tolerance of 5%. The modeling error control methodology predicts need of *LM*2222 model in the dark shaded region as shown

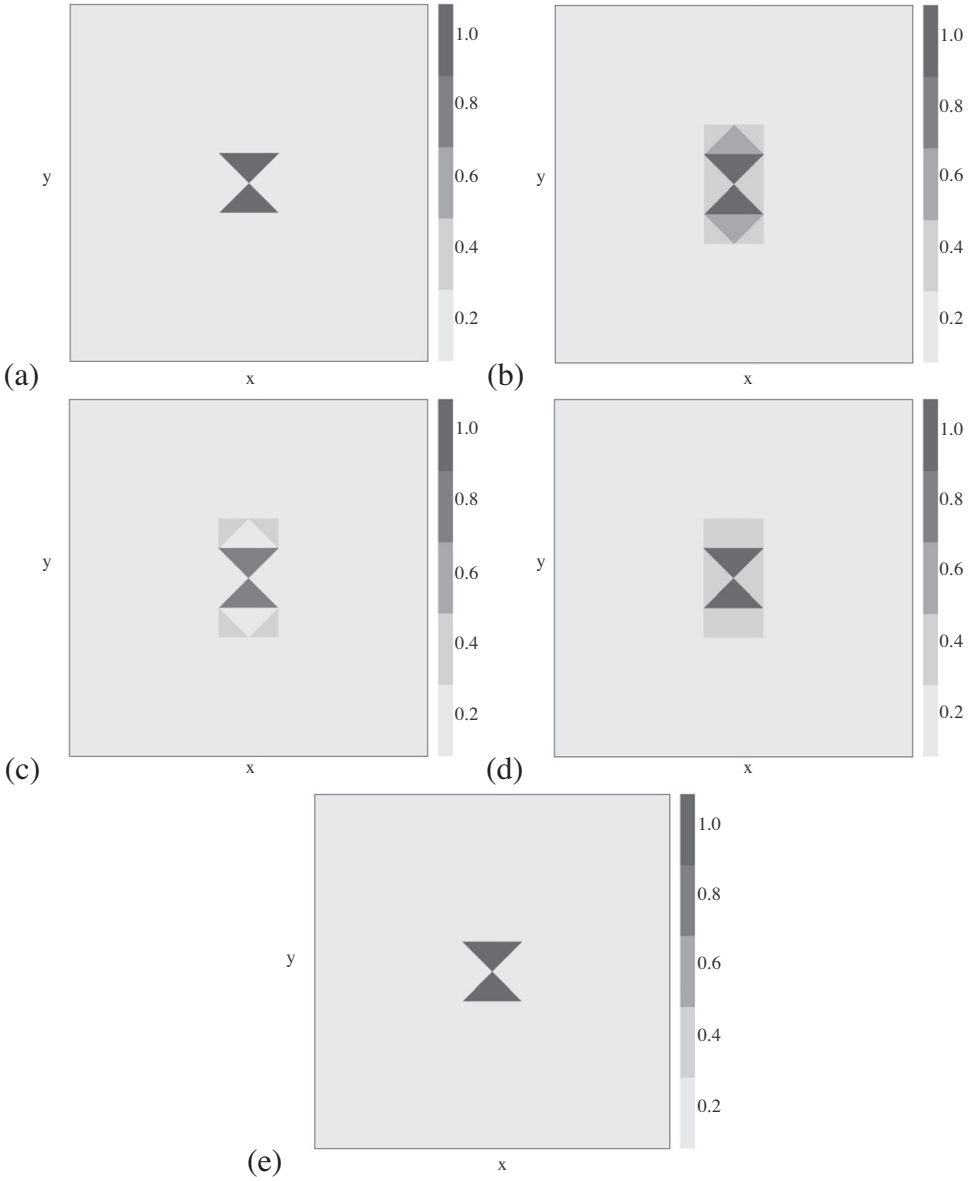

Fig. 15. Distribution of scaled modeling error energy for fiber breakage damage for the steps (a) *EQ*3332 model everywhere; (b) *LM*3332 model shown shaded as in Fig. 16(a); (c) and (d) *LM*3332 model shown shaded as in Fig. 16(b) in first and second sublayers; (e) *LM*3332 model shown shaded as in Fig. 16(c) in topmost sublayer.

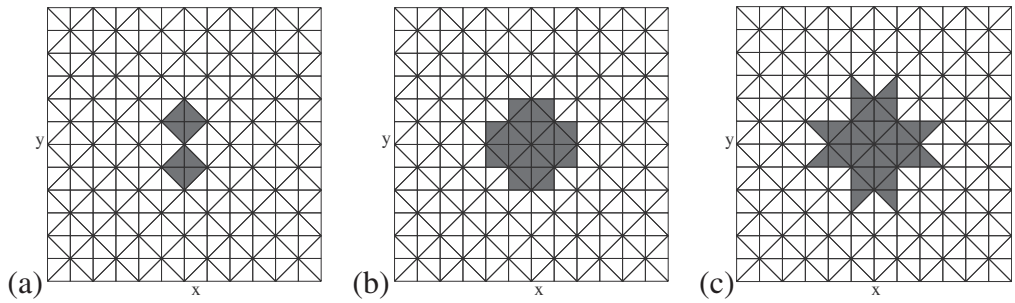

Fig. 16. Region-by-region models adapted in fiber breakage damage (shaded region shows corresponding *LM* model) in (a) step 2; (b) step 3; (c) step 4.

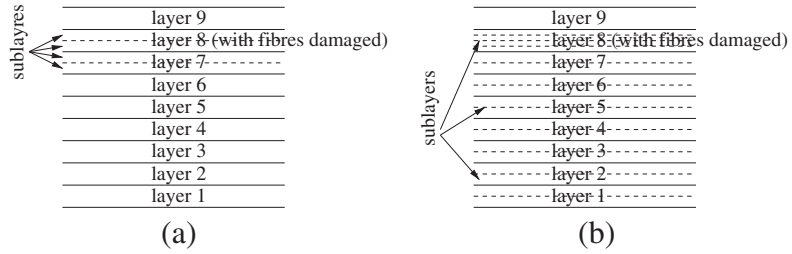

Fig. 17. Schematic representation of modeling adaptivity with sublayers in the laminate [0/90/0/90/0/90/0/90/0] with fiber damage in top-most 90° layer under uniform transverse load (see Fig. 15).

Table 10
Study of discretization and modeling error estimation and control under matrix cracking; delamination and fiber breakage static damage. The models adapted are shown in Figs. 16 and 17.

Damage	Steps	Model	Θ %	Θ_M %	$2\mathcal{U}$
Matrix cracking	1	*EQ*3332 everywhere	2.19×10^{-3}	5.37	4.40
Delamination	1	*EQ*3332 everywhere	1.95×10^{-3}	2.43	4.54
	1	*EQ*3332 everywhere	0.02	64.58	4.53
	2	*EQ*3332 + *LM*3332 Fig. 16(a)		33.93	4.53
Fiber breakage	3	*EQ*3332 + *LM*3332 with 11 layers (layers 7, 8 divided into two sublayers) Figs. 16(b) and 17(a)		25.04	4.52
	4	*EQ*3332 + *LM*3332 with 19 layers (except layer 9, all layers into sublayers. Layer 8 divided into four sublayers) Figs. 16(c) and 17(b)		17.82	4.52

in Fig. 18(c). The distribution of scaled modeling error in 90° layer for the laminate model *EQ*2222 in all the domain and mesh in Fig. 18(b) is shown in Fig. 18(d). It is clear from Fig. 18(c) that almost all the domain needs a layerwise model. The modeling error tolerance achieved with this mesh and laminate model is 3.78% and the new distribution of scaled modeling error in 90° layer is shown in Fig. 18(e). The modeling error in top and bottom layers is very low. Hence, it is not shown here. The model in Fig. 18(c) is then used to find the through thickness state of stress at (19.6875, 14.0625) in the domain. It should be noted that this point is very close to the damage front.

The same has been implemented in commercial finite element software Abaqus/Standard, that is, Abaqus Implicit (see [48]). In the damaged region of the layer a different material property has been used with $E_1^d = 0.2E_1$. The other properties are same. The mesh used in this analysis is equivalent to the mesh obtained in Fig. 18(b). Here, a hexahedral mesh with quadratic solid elements (in Abaqus it is termed as *C*3*D*20) are used in each layer for the whole domain. Note that *C*3*D*20 uses reduced integration. The number of unknowns in our model used (20073) are close to the unknowns in the model implemented using Abaqus (17835). Thus, the two analyses are equivalent. The through thickness state of stress at (19.6875, 14.0625) in the domain, obtained by both analyses is reported in Fig. 19. It should be noted that in case of Abaqus analysis the pointwise stress data is available only at specified points, like centroid of the element, integration points and unique nodal values. Here, the values at the centroid of the element (and center of the ply thickness) are used. Fig. 19(a) shows the through thickness variation of σ_{xx}. The variation of transverse normal (σ_{zz}) and shear (τ_{yz},τ_{xz}) stresses are shown in Fig. 19(b)–(d), respectively. The transverse stress components are obtained by using equilibrium equations based post-processing in the adaptive analysis. From this study it can be observed that:

1. The proposed algorithm gives a detailed map of distribution of discretization and modeling errors and adapts the mesh and model according to desired error tolerances. This feature is not found in commercial codes.
2. The proposed approach allows automatic refinement of analysis in critical region.

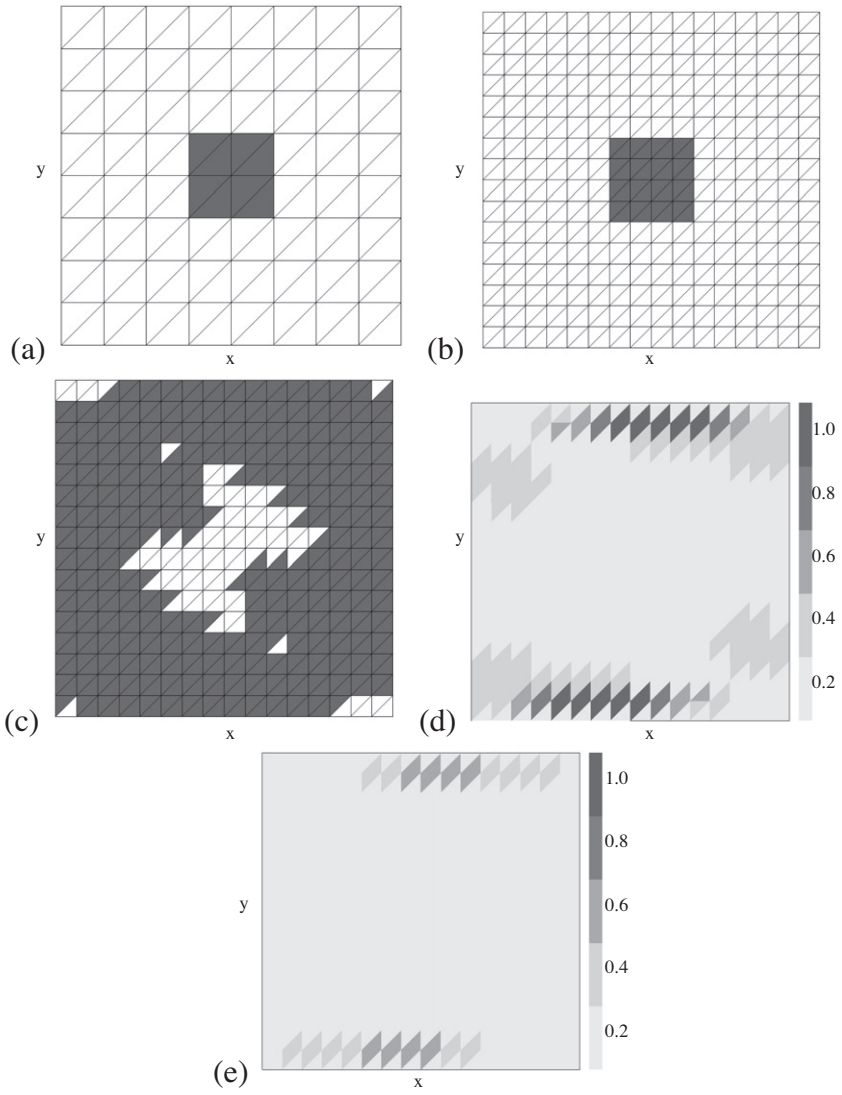

Fig. 18. Meshes used and distribution of scaled modeling error for [0/90/0] laminate with fiber breaking damage in 90° layer. (a) Initial mesh used (discretization error = 6.67%) with dark shading showing fiber breaking damage area; (b) final mesh (discretization error controlled to 0.55%) with dark shading showing fiber breaking damage area; (c) darker region showing the *LM*2222 model in the domain; (d) distribution of scaled modeling error with mesh in (b) and *EQ*2222 model everywhere in the domain; (e) distribution of scaled modeling error with mesh in (b) and *LM*2222 model as in (c). The remaining region has *EQ*2222 model.

3. The pointwise stresses, as reported in Fig. 19, show that the adopted analysis and Abaqus results are close for the inplane stress component (σ_{xx}). However, for the transverse normal and shear stress components Abaqus results show significant difference for the stress values in the damaged 90° layer. The value of the stress component σ_{zz} computed from the adaptive analysis on the top surface of the laminate (0.85 N/mm^2), where the load is applied, is close to the value of the load applied, that is 1 N/mm^2, whereas the value obtained from Abaqus is very far. Further, for transverse shear stress components obtained by adaptive analysis the variation in thickness direction is consistent.
Note that the point where these stresses are obtained is very close to the damage front and thus the through thickness variation of these stresses is expected to be significantly influenced by the damage. The Abaqus analysis seems to degrade due to this effect. The example clearly illustrates the advantage of given adaptive analysis strategy.

Remark. In the present Abaqus implementation the mesh used is given by the adaptive analysis. Further, the adaptive analysis predicted layerwise model almost everywhere in the domain. Hence, in the Abaqus the 3*D* model is used in the whole domain. Thus, the mesh and model chosen in Abaqus analysis is driven by the present adaptive analysis with the idea that both analyses are equivalent.

The goal of this study is to show that the present approach is computationally economical and accurate. The advantage of our approach is that a non-expert user can start the analysis with a crude mesh and a model, that is, an equivalent single layer model. The present approach will choose the mesh after selective refinements to achieve the user defined tolerance in the discretization error and then the proper models are adapted in different regions of the plate, if needed. To the authors knowledge, the capability of adaptive selection of models in different regions of the laminated plate is not available in any commercial finite element software.

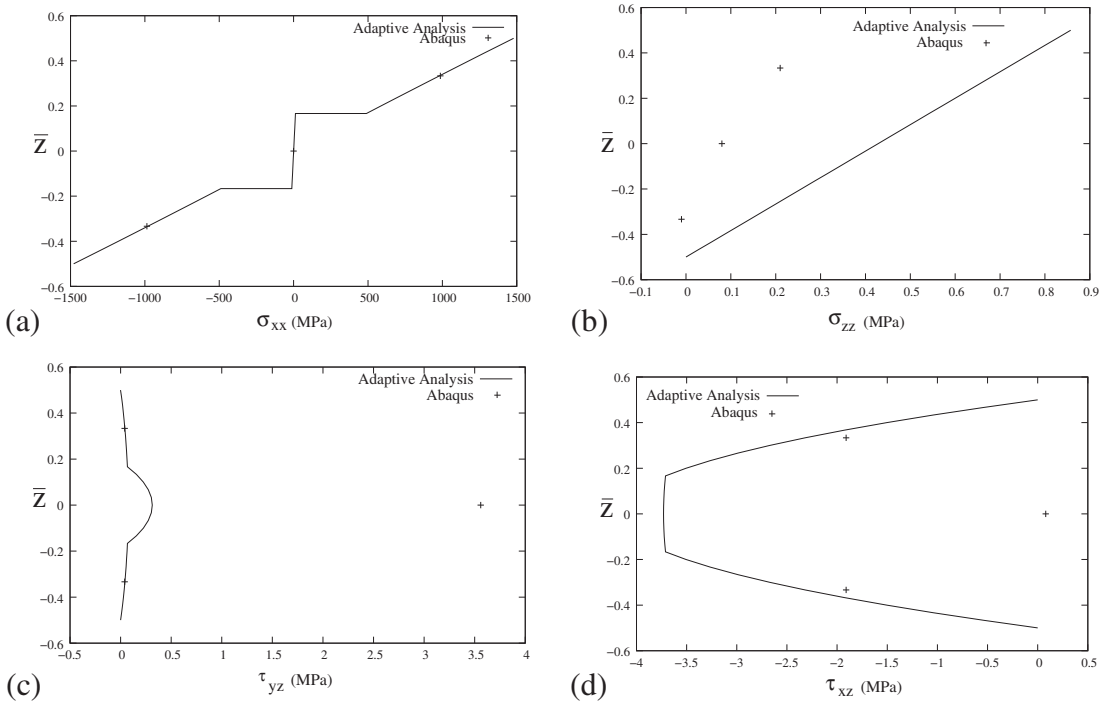

Fig. 19. Comparison of through thickness variation of stress components by adaptive analysis and Abaqus/Standard at point (19.6875,14.0625) in [0/90/0] laminate with fiber breaking damage in 90° layer. The transverse normal and shear stress components shown for the adaptive analysis are obtained by using equilibrium equations based post-processing. (a) σ_{xx}; (b) σ_{zz}; (c) τ_{yz}; (d) τ_{xz}.

Remark. Here, we have not compared the computational time taken by each approach as the current computational implementation is not optimized from an algorithmic and hardware resource usage point of view.

9. Conclusions

In the present study a generalized finite element analysis of laminated composite plates has been presented. An attempt has been made to estimate and control both discretization and modeling error. The equivalent single layer, layerwise and region-by-region plate models developed by authors earlier for laminated composites have been used. Further, the recovery based discretization error estimators developed earlier for the error in the quantity of interest or energy norm and one shot adaptivity are used to estimate and control the discretization error. An explicit modeling error indicator is proposed and implemented successfully. The proposed modeling error indicator uses the equilibrium equations based post-processed transverse stresses. Further, a systematic methodology is proposed for modeling error control. The quality of the proposed modeling error estimator is demonstrated for two values of plate length to thickness ratios, boundary conditions and lamina stacking sequences of laminate under uniform transverse load. The efficacy of the proposed approach in estimating and controlling the modeling error is also demonstrated for a cross ply symmetric laminate with different static damage modes. The results are also compared with Abaqus/Standard for accuracy and consistency. The main advantage of the proposed approach is that a non-expert user can get the desired mesh and models in the laminate automatically by the present approach to achieve the user specified error tolerances in discretization and modeling errors. Further, the present approach ensures the accurate computation of critical quantities in region of interest in one single analysis thus saving the cost and time associated with the (mesh and model) sensitivity analyses.

The main features of this study are summarized as follows:

1. The in-plane stress components are accurately computed by all models. The layerwise model accurately computes both in-plane and transverse stress components. The equilibrium equations based post-processing approach used to extract transverse stresses is effective for all models.
2. The region-by-region modeling approach is as accurate as layerwise model and computationally very economical. For the examples studied the saving in computational cost over the layerwise (or 3*D*) model can be up to 75–80%.
3. The global quality of the discretization error indicator is demonstrated for cross-ply and angle ply laminates with two different boundary conditions of clamped and soft simple support. The study is carried out for equivalent single layer and layerwise models. The estimator is found to be reliable with global effectivity index varying between 1.06 and 1.35.
4. The global quality of modeling error indicator is tested for cross-ply and angle ply anti-symmetric laminates for clamped and soft simple supported boundary conditions. The estimator is found to be good for soft simple supported conditions and can overestimate in case of clamped boundary conditions. Further, with mesh size approaching the thickness of the lamina the indicator showed improvement in quality. Overall, the indicator is found to be robust.
5. The indicator is efficient in predicting the modeling error. The modeling error indicator gives smaller errors as it uses the equilibrium equations based post-processed stress for the computation of error.
6. The proposed modeling error estimator accurately captures the plate paradox for hard simple support boundary condition.
7. The fiber damage has significant effect over matrix cracking and delamination damage for discretization and modeling error. For the problems studied the given mesh and model

were sufficient for matrix cracking and delamination damage case to have discretization and modeling error within user specified tolerance, whereas for fiber damage case the given model is not sufficient to control the specified modeling error tolerance. It required enrichment of model locally and division of layers into sublayers near the damage. This is an example of automatic adaptivity in the thickness direction. This feature is a significant contribution of this study.

8. The concept of sublayers is very effective in controlling the modeling error. For the problems studied, it reduced the modeling error by 50% in two sublayer enrichments.
9. The proposed modeling error control methodology is found to be efficient in controlling the error.
10. A non-expert user can use this approach for reliable analysis of laminates for any engineering quantity of interest. This feature will allow an analyst to obtain reliable values of all desired response quantities, hence improving confidence in computational results.

References

[1] Babuška I, Strouboulis T. The finite element method and its reliability. Oxford: Oxford Science Publications; 2001.
[2] Verfürth R. A review of a-posteriori error estimation and adaptive mesh-refinement. New York: Wiley Tuebner; 1996.
[3] Verfürth R. A review of a-posteriori error estimation techniques for elasticity problems. Comput Methods Appl Mech Eng 1999;176:419–40.
[4] Zienkiewicz OC, Zhu JZ. A simple error estimator and the adaptive procedure for practical engineering analysis. Int J Numer Methods Eng 1987;24:337–57.
[5] Zienkiewicz OC, Zhu JZ. The superconvergent patch recovery and a posteriori error estimates. Part 1: The recovery technique. Int J Numer Methods Eng 1992;33:1331–64.
[6] Mohite PM, Upadhyay CS. Local quality of smoothening based a-posteriori error estimators for laminated plates under transverse loading. Comput Struct 2002;80(18–19):1477–88.
[7] Mohite PM, Upadhyay CS. Focussed adaptivity for laminated plates. Comput Struct 2003;81(5):287–98.
[8] Mohite PM, Upadhyay CS. Reliable computation of local quantities of interest in composite laminated plates. In: 47th AIAA/ASME/ASCE/AHS/ASC structures, structural dynamics and materials conference, Rhode Island, USA; 2006. p. 365–85.
[9] Mohite PM, Upadhyay CS. Accurate computation of critical local quantities in composite laminate plates under transverse loading. Comput Struct 2006;84:657–75.
[10] Mohite PM. A generalized adaptive finite element modeling based analysis of undamaged and damaged laminated composite structures. PhD thesis, Indian Institute of Technology Kanpur, India; 2006.
[11] Grätsch T, Bathe KJ. A posteriori error estimation techniques in practical finite element analysis. Comput Struct 2005;83:235–65.
[12] Actis RL, Szabó BA, Schwab C. Hierarchic models for laminated plates and shells. Comput Methods Appl Mech Eng 1999;172:79–107.
[13] Vogelius M, Babuška I. On a dimensional reduction method: III. A-posteriori error estimation and adaptive approach. Math Comput 1981;37(156):361–84.
[14] Babuška I, Schwab C. A-posteriori error estimation for hierarchic models of elliptic boundary value problem on thin domains. Technical note BN-1148. Institute for Physical Science and Technology, University of Maryland, College Park; 1993.
[15] Oden JT, Cho JR. Adaptive *hpq*-finite element methods of hierarchical models for plate- and shell-like structures. Comput Methods Appl Mech Eng 1996;136(3–4):317–45.
[16] Stein E, Rust W, Ohnimus S. *h* and *d* adaptive FE methods for two-dimensional structural problems including post-buckling of shells. Comput Methods Appl Mech Eng 1992;101:315–54.
[17] Stein E, Ohnimus S. Coupled model and solution-adaptivity in the finite element method. Comput Methods Appl Mech Eng 1997;150:327–50.
[18] Stein E, Ohnimus S. Anisotropic discretization and model-error estimation in solid mechanics by local Neumann problem. Comput Methods Appl Mech Eng 1999;176:363–85.
[19] Oden JT, Vemaganti KS, Moës N. Hierarchical modeling of heterogeneous solids. Comput Methods Appl Mech Eng 1999;172:3–25.
[20] Vemaganti KS, Oden JT. Estimation of local modeling error and goal-oriented adaptive modeling of heterogeneous materials. Part I: Error estimates and adptive algorithms. J Comput Phys 2000;164:22–47.
[21] Vemaganti KS, Oden JT. Estimation of local modeling error and goal-oriented adaptive modeling of heterogeneous materials. Part II: A computational environment for adaptive modeling of heterogeneous elastic solids. Comput Methods Appl Mech Eng 2001;190:6089–124.
[22] Schwab C. A-posteriori modeling error estimation for hierarchic plate model. Numer Math 1996;74:221–59.
[23] Babuška I, Schwab C. A-posteriori error estimation for hierarchic models of elliptic boundary value problems on thin domains. SIAM J Numer Anal 1996;23(1):221–46.
[24] Babuška I, Schwab C. On the a-posteriori estimation of the modeling error for the heat conduction in a plate and its use for adaptive hierarchical modeling. Appl Numer Math 1994;4:5–21.
[25] Oden JT, Prudhomme S. Estimation of modeling error in computational mechanics. J Comput Phys 2002;182:496–515.
[26] Mohite PM, Upadhyay CS. A novel subdomainwise modeling approach for analysis of layered composite structures. In: 48th AIAA/ASME/ASCE/AHS/ASC structures, structural dynamics and materials conference, Honolulu, Hawaii, USA; 2006.
[27] Mohite PM, Upadhyay CS. Region-by-region modeling of laminates composite plates. Comput Struct 2007;85. p. 23–4, 1808–27.
[28] Reddy JN. Mechanics of laminated composite plates and shells. 2nd ed. Boca Raton, USA: CRC Press; 2004.
[29] Carrera E. Historical review of zig-zag theories for multilayered plate and shells. Appl Mech Rev 2003;56(3):287–308.
[30] Babuška I, Strouboulis T, Mathur A, Upadhyay CS. Pollution error in the *h* version of the finite element method and the local quality of a-posteriori error estimators. Finite Elem Anal Des 1994;17:273–321.
[31] Babuška I, Strouboulis T, Upadhyay CS. A model study of the quality of a-posteriori error estimators for linear elliptic problems. Error estimation in the interior of patchwise uniform grids of triangles. Comput Methods Appl Mech Eng 1994;114:307–78.
[32] Babuška I, Upadhyay CS, Gangaraj SK, Copps K. Validation of a-posteriori error estimators by numerical approach. Int J Numer Methods Eng 1994;37:1073–123.
[33] Reddy YSN, Reddy JN. Linear and non-linear failure analysis of composite laminates with transverse shear. Compos Sci Technol 1992;44:227–55.
[34] Ladevéze P. A damage computational method for composite structures. Comput Struct 1992;44(1):79–87.
[35] Ladevéze P, Dantec Le. Damage modeling of elementary ply for laminated composites. Compos Sci Technol 1992;43:257–67.
[36] Allix O, Ladevéze P, Vittecoq E. Modeling and identification of the mechanical behaviour of composite laminates in compression. Compos Sci Technol 1994;51:35–42.
[37] Allix O, Ladevéze P. Interlaminar interface modelling for the prediction of delamination. Compos Struct 1992;22:235–42.
[38] Allix O, Ladevéze P, Corigliano A. Damage analysis of interlaminar fracture specimens. Compos Struct 1995;31:61–74.
[39] Allix O, évêque DL, Perret L. Identification and forecast of delamination in composite laminates by an interlaminar interface model. Compos Sci Technol 1998;58:641–78.
[40] Babuška I, Strouboulis T, Upadhyay CS, Gangaraj SK. A-Posteriori estimation and adaptive control of the pollution error in the h version of the finite element method. Int J Numer Methods Eng 1995;38:4207–35.
[41] Wahlbin LB. Local behavior in finite element methods. In: Ciarlet PG, Lions JL, editors. Handbook of numerical analysis, vol. 2. North Holland; 1991. p. 357–521.
[42] Ladevèze P, Pelle JP, Rougeot PH. Error estimation and mesh optimization for classical finite elements. Eng Comput 1991;8:69–80.
[43] Pagano NJ, Hatfield SJ. Elastic behavior of multilayered bidirectional composites. AIAA J 1972;10(7):931–3.
[44] Babuška I, Pitkäranta J. The plate paradox for hard and simple support. SIAM J Math Anal 1990;21(3):551–76.
[45] Babuška I, Li L. Hierarchic modeling of plates. Comput Struct 1991;40(2):419–30.
[46] Babuška I, Li L. The problem of plate modeling: theoretical and computational results. Comput Methods Appl Mech Eng 1992;100:249–73.
[47] Babuška I, Scapolla T. Benchmark computation and performance evaluation for a rhombic plate bending problem. Int J Numer Methods Eng 1989;28:155–79.
[48] Abaqus 6.10 Documentation.